

# Causal Discovery from Time Series with Hybrids of Constraint-Based and Noise-Based Algorithms

Anonymous authors

Paper under double-blind review

## Abstract

Constraint-based methods and noise-based methods are two distinct families of methods proposed for uncovering causal graphs from observational data. However, both operate under strong assumptions that may be challenging to validate or could be violated in real-world scenarios. In response to these challenges, there is a growing interest in hybrid methods that amalgamate principles from both methods, showing robustness to assumption violations. This paper introduces a novel comprehensive framework for hybridizing constraint-based and noise-based methods designed to uncover causal graphs from observational time series. The framework is structured into two classes. The first class employs a noise-based strategy to identify a super graph, containing the true graph, followed by a constraint-based strategy to eliminate unnecessary edges. In the second class, a constraint-based strategy is applied to identify a skeleton, which is then oriented using a noise-based strategy. The paper provides theoretical guarantees for each class under the condition that all assumptions are satisfied, and it outlines some properties when assumptions are violated. To validate the efficacy of the framework, two algorithms from each class are experimentally tested on simulated data, realistic ecological data, and real datasets sourced from diverse applications. Notably, two novel datasets related to Information Technology monitoring are introduced within the set of considered real datasets. The experimental results underscore the robustness and effectiveness of the hybrid approaches across a broad spectrum of datasets.

## 1 Introduction

Recent technological advances allow collecting observational time series on complex dynamical systems in various fields, such as biodiversity monitoring in ecology (Dornelas et al., 2018), healthcare (Morid et al., 2023), and Information Technology (IT) monitoring systems (Tamburri et al., 2020, Assaad et al., 2023). One of the key objectives in studying such dynamical systems is to understand the causal relationships between the system’s components. To find these causal relations, experts can employ causal discovery methods for time series, which aim to build a causal graph from observational data. These methods can be categorized into several families, including Granger (Granger, 1969), constraint-based (Spirtes et al., 2000, Runge, 2020, Assaad et al., 2022c), score-based (Chickering, 2002b) and noise-based families (Hyvärinen et al., 2008, Peters et al., 2013) —for more details see Assaad et al. (2022a), Hasan et al. (2023), Gong et al. (2023). Each family has its own set of assumptions, which may or may not be suitable for a specific dataset. Therefore, no single method stands out in all situations (Assaad et al., 2022a).

Hybrid frameworks combine several methods from different families to enhance graph inference (Hasan et al., 2023). For non-temporal data, several authors propose to combine ideas from constraint-based and score-based methods to improve scalability (Tsamardinos et al., 2006) or robustness to small sample size (Ogarrio et al., 2016). For temporal data, SVAR-GFCI, proposed by Malinsky & Spirtes (2018), is a time-series generalization of the hybrid method GFCI which is based on the score-based and constraint-based algorithms.

Another type of hybrid framework, which is our main focus in this work, is based on the combination of constraint-based and noise-based families. The advantage of constraint-based methods is that they are

non-parametric (i.e., no assumption is made on the form of the underlying causal relationships), while the limitation is that they require strong non-testable assumptions and can only recover the causal graph up to its Markov equivalence class, i.e., orientation of some edges could be unknown in the inferred graph as several graphs represent the same conditional dependence structure. On the other hand, noise-based methods are capable of recovering true graphs. So, by combining methods from both families, although we require assumptions of both families of methods, some assumptions can be weakened and we can recover the true causal graph. There exist several methods of this type for non-temporal data, such as PClingam (Hoyer et al., 2008) or FRITL (Chen et al., 2021). Assaad et al. (2021) introduced NBCB<sup>acyclic</sup><sup>1</sup> for temporal data assuming that there are no cycles in the causal graph between the time series.

This paper presents a hybrid framework for temporal data using noise-based and constraint-based algorithms. In this framework, we consider two different classes of methods, which we denote NBCB and CBNB. Both classes can infer different types of causal graphs that differentiate between instantaneous relations and lagged relations. To construct these types of causal graphs, NBCB and CBNB orient edges using a noise-based strategy and prune edges using a constraint-based strategy. The main difference between NBCB and CBNB is that the former starts by orienting the graph and then proceeds to pruning, while the latter starts by pruning and then proceeds to orientation. Most, importantly, NBCB and CBNB combine the parts from corresponding methods in an efficient way, such that information in the first part improves the efficiency of the second part. At the core of CBNB lies the notion of an undirected cycle group, which we introduce to optimize the search for orientation.

Our main contributions are:

- We propose a hybrid framework for the causal discovery of time series that combines parts of noise-based and constraint-based algorithms. Within this framework, we derive two classes of algorithms, NBCB and CBNB, which we optimize to infer the causal graph from time series.
- We study theoretically to which extent each class of algorithms is robust against assumption violation.
- We provide extensive simulation studies and real data applications to illustrate the applicability of our approach and their enhanced capabilities against assumption violation compared to original methods.
- We introduce two novel datasets about IT monitoring within the set of considered real datasets.

The remainder of the paper is organized as follows: Section 2 describes the different types of causal graphs that can be used to represent causal relations between time series and the different assumptions related to those graphs. Section 3 discusses related work and particularly details the steps that compose noise-based and constraint-based algorithms. Section 4 introduces our main contribution, the hybrid framework, which consists of two classes NBCB and CBNB, each of which is detailed in dedicated subsections. In Section 5, NBCB and CBNB are compared to different causal discovery algorithms on simulated, realistic, and real datasets. Finally, Sections 6 and 7 discuss and conclude the paper.

## 2 Background

In this section, we first introduce some terminology, tools, and assumptions which are standard for the major part. We use upper case letters to denote observed random variables, lower case letters to represent deterministic constants, blackboard bold for sets, and Greek letter  $\xi$  to denote noise. A graph is denoted as  $\mathcal{G}$  and parents and descendants of  $X$  in  $\mathcal{G}$  are respectively denoted as  $\text{Pa}_{\mathcal{G}}(X)$  and  $\text{Desc}_{\mathcal{G}}(X)$ . We denote  $\langle X, \dots, Y \rangle$  as a path in a graph which starts at node  $X$  and end at node  $Y$ .

Causal relations in a dynamical system can be represented by a dynamic structural causal model, an extension of structural causal model (SCM, Pearl, 2000) to time series. Without loss of generality, we will use the linear dynamic SCM represented in Equation (1) as a running example.

<sup>1</sup>In Assaad et al. (2021), this method was called NBCB but in this work, we denote it as NBCB<sup>acyclic</sup> to explicitly point out that it assumes that the summary causal graph is acyclic.

$$\begin{aligned}
X_t &:= a_x X_{t-1} + a_{y x} Y_t + a_{z x} Z_t + \xi_t^x \\
Z_t &:= a_z Z_{t-1} + a_{x z} X_{t-1} + a_{y z} Y_t + a_{w z} W_{t-1} + \xi_t^z \\
Y_t &:= a_y Y_{t-1} + a_{x y} X_{t-1} + a_{w y} W_{t-2} + \xi_t^y \\
W_t &:= a_w W_{t-1} + a_{y w} Y_t + a_{z w} Z_t + \xi_t^w \\
U_t &:= a_u U_{t-1} + a_{w u} W_t + \xi_t^u.
\end{aligned}
\tag{1}$$

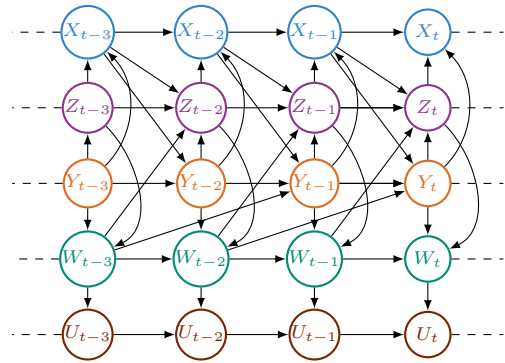


Figure 1: Running example. Left: Dynamic structural causal model (dynamic SCM). Right: Associated full-time causal graph  $\mathcal{G}$  (FTCG).

Such a dynamic SCM can be represented graphically using a full-time causal graph (FTCG) (Assaad et al., 2022a), as represented in Figure 1. The full-time causal graph denoted as  $\mathcal{G}^f = (\mathbb{E}^f, \mathbb{V}^f)$  represents an infinite graph of the dynamical system through infinite nodes  $\mathbb{V}^f$ , representing observed random variables, and infinite edges  $\mathbb{E}^f$ . We can also consider the skeleton graph, which contains only undirected edges that represent adjacencies in graph  $\mathcal{G}^f$  (Hasan et al., 2023).

## 2.1 Assumptions

One of the most common assumptions is the causal Markov condition, which is assumed by most of the methods, and connects the causal graphs that correspond to the given SCM with the compatible probability distributions.

**Assumption 1** (Causal Markov Condition, [Spirtes et al., 2000](#)). Let  $\mathcal{G}$  be a causal graph with vertex set  $\mathbb{V}$  and  $P$  be a probability distribution over the vertices in  $\mathbb{V}$  generated by the causal structure represented by  $\mathcal{G}$ . Every  $X \in \mathbb{V}$  is independent of  $\mathbb{V} \setminus \{\text{Desc}_{\mathcal{G}}(X) \cup \text{Pa}_{\mathcal{G}}(X)\}$  given  $\text{Pa}_{\mathcal{G}}(X)$ .

We assume that there are no hidden common causes, an assumption known as causal sufficiency.

**Assumption 2** (Causal Sufficiency, [Spirtes et al., 2000](#)). *There exist no hidden common causes of any two observed nodes, i.e., the noise terms in the underlying dynamic SCM are jointly independent.*

In general, inference of causal graphs from data is possible under additional assumptions on the data-generating process. For the constraint-based family of methods, the necessary assumption for the correspondence between the graph and the distribution is the faithfulness assumption (Spirtes et al., 2000), which states that all the conditional independence relations that are true in the probability distribution are entailed by the Markov condition applied to  $\mathcal{G}$ . However, we consider in this work the following weaker version of the faithfulness assumption, called adjacency faithfulness.

**Assumption 3** (Adjacency Faithfulness, [Ramsey et al., 2006](#)). *Let  $\mathcal{G}$  be a causal graph with vertex set  $\mathbb{V}$ . If two vertices  $X$  and  $Y$  are adjacent in  $\mathcal{G}$ , then they are dependent conditional on any subset of  $\mathbb{V} \setminus \{X, Y\}$ .*

Note that adjacency faithfulness is proven to be equivalent to the minimality condition (Peters et al., 2017) introduced in Spirtes et al. (2000), which states that every proper subgraph of  $\mathcal{G}$  does not satisfy causal Markov condition.

In addition, the following assumption is required by the noise-based family to guarantee identifiability.

**Assumption 4** (Identifiable Functional Model, [Peters et al., 2011](#)). *The data generating mechanism belongs to an identifiable functional model class, as defined in [Peters et al. \(2011\)](#).*

For example, the linear dynamic SCM in Equation (1) satisfies Assumption 4 if the noise terms are non-Gaussian.

Finally, the following assumption is required to recover the proper graph.

**Assumption 5** (Acyclicity). *Let  $\mathcal{G}$  be a causal graph. There exists no directed path in  $\mathcal{G}$  that starts and ends at the same node.*

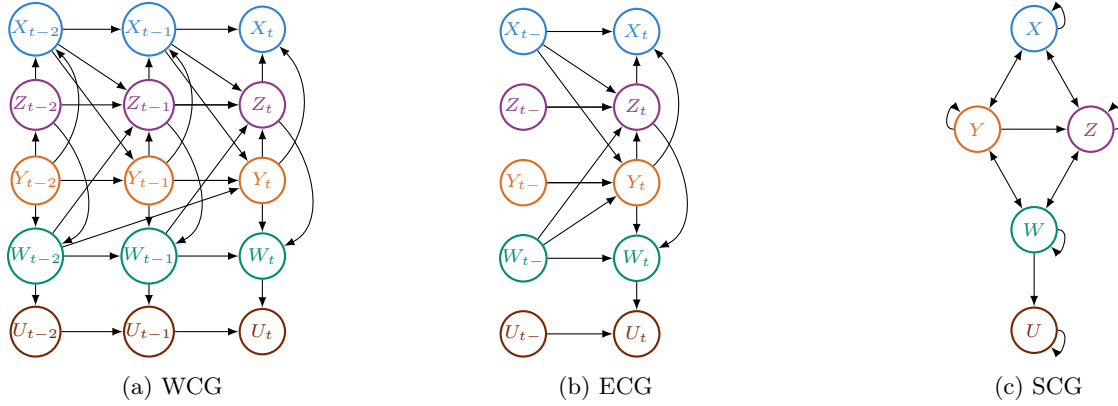


Figure 2: Different causal graphs to represent the dynamic SCM in Equation (1): (a) window causal graph (WCG) with a maximal temporal lag equal to 2, (b) extended summary causal graph (ECG), and (c) summary causal graph (SCG).

## 2.2 Causal graphs for time series

Using time series data has a particular advantage for discovering causal relationships between temporal variables since we can employ temporal priority, which states that the causal relationship between two variables is oriented such that the effect cannot happen before its cause. However, despite this advantage, working with full-time causal graphs (which was introduced before) is impractical due to their infinite dimension, which has led to the adoption of simpler causal graphs, assuming that causal relations between time series hold throughout time. This is formalized in the following assumption, in which  $\mathbb{V}^f = (\mathbb{V}_{-\infty}, \dots, \mathbb{V}_t, \dots, \mathbb{V}_{\infty})$  where  $\mathbb{V}$  denotes a vector of  $d$  time series.

**Assumption 6** (Consistency Throughout Time). *Let  $\mathcal{G}^f = (\mathbb{E}^f, \mathbb{V}^f)$  be a full-time causal graph. There exists  $\gamma$  in  $\mathbb{N}^*$  such that the causal structure of the graph consisting of the nodes  $\{\mathbb{V}_{t-\gamma}, \dots, \mathbb{V}_t\}$  is the same for every  $t$ .*

We call the minimum value of  $\gamma$  for which consistency throughout time holds the *maximal temporal lag* of the graph. For example, the maximal temporal lag of the graph of Figure 1 is  $\gamma = 2$ .

Under Assumption 6, the full-time causal graph is equivalent to the so-called window causal graph (Hyvärinen et al., 2008, Runge, 2020, Figure 2a).

**Definition 1** (Window Causal Graph, WCG). *Let  $\mathcal{G}^f = (\mathbb{E}^f, \mathbb{V}^f)$  be a full-time causal graph satisfying Assumption 6 with  $\gamma$  the maximal temporal lag in  $\mathcal{G}^f$ . A window causal graph (WCG)  $\mathcal{G}^w = (\mathbb{E}^w, \mathbb{V}^w)$  is the subgraph of  $\mathcal{G}^f$  consisting of the nodes  $\mathbb{V}^w = (\mathbb{V}_{t-\gamma}, \dots, \mathbb{V}_t)$  and  $\mathbb{E}^w$  contains all related edges.*

Unfortunately, causal discovery methods still suffer in practice of the strong assumptions they rely on that are not always satisfied. Thus, in many applications, experts have to validate those graphs before using them. However, validating WCGs is challenging: if they can usually identify causes and related effects, they do not know, in general, the exact temporal lags between them. Moreover, in some applications, experts are not interested in understanding exact causal relations with the temporal lags between them but rather opt for an abstract representation of the causal relationships between variables by using a summary causal graph (Arnold et al., 2007, Peters et al., 2013, Assaad et al., 2022a, Figure 2c), which provides an overview of the causal relationships between time series without delving into the details of their specific temporal relationships.

**Definition 2** (Summary Causal Graph, SCG). *Let  $\mathcal{G}^w = (\mathbb{E}^w, \mathbb{V}^w)$  be a WCG with maximal temporal lag  $\gamma$ . The underlying summary causal graph (SCG) of  $\mathcal{G}^w$  is  $\mathcal{G}^s = (\mathbb{E}^s, \mathbb{V}^s)$  where  $\mathbb{V}^s$  contains one node for each time series and the set of directed edges  $\mathbb{E}^s$  are defined as follows: for all  $X, Y \in \mathbb{V}^s$ ,  $X \neq Y$ , there exists a directed edge from  $X$  to  $Y$  (denoted as  $X \rightarrow Y$ ) if and only if there exists at least one temporal lag  $\ell \geq 0$  such that there exists a directed edge between  $X_{t-\ell}$  and  $Y_t$  in  $\mathcal{G}^w$ .*

Summary causal graphs have proved to be useful in many applications. However, to discover the summary causal graph from data it is often necessary to infer the window causal graph, from which the summary causal

graph is further deduced or make additional assumptions. An extended summary causal graph (Assaad et al., 2022c, Figure 2b), serves as a compromise between the summary and window causal graphs and is a type of abstraction that differentiates between instantaneous relations and lagged relations without giving precise information about the lag. Thus unlike summary causal graphs, it can be directly discovered from the data without additional assumptions.

**Definition 3** (Extended Summary Causal Graph, ECG). *Let  $\mathcal{G}^w = (\mathbb{E}^w, \mathbb{V}^w)$  be a WCG with maximal temporal lag  $\gamma$  and nodes  $(\mathbb{V}_{t-\gamma}, \dots, \mathbb{V}_t)$ . The underlying extended summary causal graph (ECG)  $\mathcal{G}^e = (\mathbb{E}^e, \mathbb{V}^e)$  consists of the nodes  $\mathbb{V}^e = (\mathbb{V}_{t-}, \mathbb{V}_t)$  and the set of directed edges  $\mathbb{E}^e$  is defined as follows: for all  $X_t, Y_t \in \mathbb{V}_t$ ,  $X_t \neq Y_t$ , there exists a directed edge from  $X_t$  to  $Y_t$  (denoted as  $X_t \rightarrow Y_t$ ) if and only if the same directed edge exists in  $\mathcal{G}^w$ ; for all  $X_{t-} \in \mathbb{V}_{t-}, Y_t \in \mathbb{V}_t$ , there exists a directed edge from  $X_{t-}$  to  $Y_t$  (denoted as  $X_{t-} \rightarrow Y_t$ ) if and only if there exists at least one temporal lag  $\ell > 0$  such that there exists a directed edge between  $X_{t-\ell}$  and  $Y_t$  in  $\mathcal{G}^w$ .*

Remark that because the full-time causal graph is supposed to be acyclic (Assumption 5), the WCG and the ECG are also acyclic, but the SCG may be cyclic, as illustrated in the running example in Figure 2.

We use throughout for clarity the notation  $\mathcal{G}^* = (\mathbb{V}^*, \mathbb{E}^*)$  to refer to either  $\mathcal{G}^e = (\mathbb{E}^e, \mathbb{V}^e)$  or  $\mathcal{G}^w = (\mathbb{E}^w, \mathbb{V}^w)$ . Moreover, we use the notation  $t^*$  as a wildcard that represents time step  $t - i$ , where  $i \in \{0, \dots, \gamma\}$  in the context of WCG, and that represents either  $t-$  or  $t$  in the context of ECG.

Another important notion that we will use in this paper is the notion of a causal order (Peters et al., 2017) which we define, in the following, only for instantaneous nodes.

**Definition 4** (Causal Order of Instantaneous Nodes). *Given a causal graph  $\mathcal{G}^*$ , we call a bijective mapping  $\pi : \mathbb{V}_t \mapsto \{1, \dots, d\}$ , a causal order of instantaneous nodes if it satisfies*

$$\pi(X_t) < \pi(Y_t) \quad \text{if } Y_t \in \text{Desc}_{\mathcal{G}^*}(X_t), \forall X_t, Y_t \in \mathbb{V}_t.$$

Because of the acyclicity assumption of the WCG (resp. ECG), there is always a causal order between instantaneous nodes (and a fortiori between all nodes) but it is not necessarily unique (Peters et al., 2017). For example, in Figure 2a, there exists a causal order  $\pi_1$  such that  $\pi_1(X_t) = 3$  and  $\pi_1(W_t) = 4$  and there exists another causal order  $\pi_2$  such that  $\pi_2(W_t) = 3$  and  $\pi_2(X_t) = 4$ . Note that  $\pi_1(Y_t) = \pi_2(Y_t) = 1$ ,  $\pi_1(Z_t) = \pi_2(Z_t) = 2$  and  $\pi_1(U_t) = \pi_2(U_t) = 5$ .

### 3 Related works

In this section, we start by giving a general literature review and then we give additional details on the steps that compose noise-based and constraint-based algorithms.

#### 3.1 Literature review

In this section, we describe several methods from the main causal discovery families of methods related to our work. More details can be found in thorough reviews such as Assaad et al. (2022a), Hasan et al. (2023), Gong et al. (2023).

Granger Causality, introduced by Granger in 1969 and improved in subsequent works (Granger, 2004, Arnold et al., 2007), stands as one of the earliest methods designed for identifying causal relationships among time series. This approach primarily considers linear relationships and temporal priorities, operating under the assumption that the past of a cause is both necessary and sufficient for optimally forecasting its effect. It is important to note that Granger causality, by relying on temporal priority, is limited in its ability to infer instantaneous causal relations. Furthermore, Granger causality methods typically utilize the past of one time series, up to a defined maximal temporal lag, to predict the present value of another time series without explicitly distinguishing between the importance of different lags. Consequently, these methods can be employed in constructing an ECG if we assume that there is no instantaneous relations.

Constraint-based approaches (Spirtes et al., 2000) are certainly the most popular approaches for discovering causal graphs. These methods are based on conditional independence tests, do not depend on any specific distribution form, and require the faithfulness assumption. In the case of causal sufficiency (Assumption 2), they are usually based on the PC-algorithm (Spirtes et al., 2000) which was initially introduced for non-temporal data. In theory, a constraint-based algorithm can only infer a representative (known as a CPDAG, Chickering, 2002a) of the Markov equivalence class (Verma & Pearl, 1990). Fast Causal Inference (FCI)



algorithm can be used when Assumption 2 is not satisfied and infers a Partially Ancestral Graph (PAG), which is a representative of a class of equivalent Maximal ancestral graphs (MAG) and allows to represent the existence of the hidden confounders in the causal graph. For time series, several algorithms infer WCGs, such as PC-MCI (Runge et al., 2019) and PC-MCI<sup>+</sup> (Runge, 2020), extensions of the PC-algorithm and tsFCI (Entner & Hoyer, 2010) or SVAR-FCI (Malinsky & Spirtes, 2018), extensions of FCI algorithm. PCGCE proposed by Assaad et al. (2022c), is based on the adaptation of PC-algorithm and infers directly an ECG. Score-based approaches (Chickering, 2002a) search over the space of possible graphs trying to maximize a score that reflects how well the graph fits the data. Greedy Equivalence Search (GES, Chickering, 2002a) is one of the first score-based methods that, under the faithfulness assumption, find the CPDAG similarly to the PC-algorithm. There have been several recent modifications of GES such as more efficient Fast Greedy Search (FGS, Ramsey, 2015) and Selective Greedy Equivalence Search (Chickering & Meek, 2015). Recently, a new score-based method called Dynotears (Pamfil et al., 2020) was presented to infer a WCG from a time series.

Noise-based approaches discover causal relations using footprints produced by the causal asymmetry in the data, namely the noise. For time series, one of the most popular algorithms in this family is VarLiNGAM (Hyvärinen et al., 2008), which can discover the WCG assuming linear autoregressive models and non-Gaussian noise. TiMINo (Peters et al., 2013) discovers the SCG assuming a nonlinear additive noise model. Note that TiMINo only assumes non-Gaussian noise when causal relations are linear. These approaches also require the minimality condition.

Hybrid frameworks integrate methods from different families to improve inference of the graph, by mitigating the limitations of one algorithm through its combination with another algorithm. One group of methods combines constraint-based and score-based methods. Greedy Fast Causal inference (GF-CI, Ogarrio et al., 2016) is a combination of constraint-based FCI algorithm and GES algorithm, which allows to address FCI limited applicability on small sample size data and correct graph inferred by GES in the presence of latent confounders. HCM hybrid (Li et al., 2022) aims to discover the causal structure from mixed nontemporal data and combines part of the constraint-based method and greedy search adapted for mixed data. SVAR-GFCI introduced by Malinsky & Spirtes (2018) extends GF-CI for temporal data.

Another type of hybrid method is a combination of the constraint-based and noise-based methods. Hoyer et al. (2008) presented a hybrid approach called PClingam that starts with a constraint-based procedure to find the pattern of the graph and then uses a noise-based procedure to orient some of the non-oriented edges (depending on the noise distribution), which allows obtaining more informative causal graph. Another algorithm called FRITL (Chen et al., 2021), aims to infer more informative causal graphs with the presence of hidden confounders using the noise-based LiNGAM methods to refine the output of the FCI algorithm. For time series, a combination of noise-based and constraint-based methods was proposed by Assaad et al. (2021)—to infer an SCG assuming there is no cycles between different time series—which starts with inferring causal order using an additive noise model and pruning unnecessary edges using conditionally independent tests.

### 3.2 Details on noise-based and constraint-based methods

Let us first describe the basic steps of noise-based methods. A noise-based algorithm that infers a causal graph relies on the fact that, under Assumption 4, a prediction model of a target node  $Y$  where the predictors are the true causes of  $Y$  should yield residuals (that represent the noise) that are independent of the causes. The procedure of such an algorithm can be divided into two main steps:

- NB1. Find the causal order between instantaneous nodes  $\mathbb{V}_t$  by recursively performing regression and independence tests between the predictors and residuals (noise). But note that even if only instantaneous nodes  $\mathbb{V}_t$  are accounted for, lagged nodes are used in the regression as a means to account for confounder bias. For example, assuming linearity, we use the following regression model to compute the residuals of each  $Y_t \in \mathbb{V}_t$ :

$$Y_t = \sum_{X_t \in \mathbb{V}_t \setminus \{Y_t\}} a_{xy} X_t + \sum_{Z_{t-\ell} \in \mathbb{V}^* \setminus \mathbb{V}_t} a_{zy\ell} Z_{t-\ell} + \xi_t^y. \quad (2)$$

- NB2. Find which set of predictors is not needed to keep the independence between other predictors and residuals. The former set of predictors is considered as not causally related to the node that is predicted and the latter set of predictors is considered as the causes of this node.

In general, step NB1 requires only Assumptions 1, 2, 4, 5 and 6. Note that it has been shown that the causal order can be identified even if Assumption 3 is violated (Peters et al., 2014)<sup>2</sup>. However, Peters et al. (2014) only considered the identifiability of the causal order in case of violation of Assumption 3 up to the additive noise model case. Still, we expect a similar statement to hold in general for all identifiable functional models. However, Assumption 3 is required for step NB2. The output of step NB1 is a causal order  $\hat{\pi}$ . For step NB1 one can use, for example, TiMINo (Peters et al., 2013) or VarLiNGAM (Hyvärinen et al., 2008) algorithms.

Turning to constraint-based methods, we focus in this paper on the methods that are based on the PC-algorithm, which requires Assumption 2. It follows that most constraint-based algorithms for WCGs or ECGs can be divided into two main steps:

- CB1. Initialize a fully connected graph such that lagged relations are oriented using temporal priority (if  $X_{t^*}$  is adjacent to  $Y_t$  and  $t^* < t$  then  $X_{t^*} \rightarrow Y_t$ ) and instantaneous relations are unoriented, and then prune unnecessary edges using the following procedure:
  - (a) Eliminate edges between nodes  $(X_{t^*}, Y_t)$  if  $X_{t^*} \perp\!\!\!\perp Y_t$ .
  - (b) For each pair of nodes  $(X_{t^*}, Y_t)$  having an edge between them, and for each subset of nodes  $\mathbb{S} \subseteq \mathbb{V}^* \setminus \{X_{t^*}, Y_t\}$  of size  $n = 1$  such that  $\forall Z_{t'} \in \mathbb{S}$ ,  $Z_{t'}$  is adjacent to  $Y_t$ , eliminate the edge between  $X_{t^*}$  and  $Y_t$  if  $X_{t^*} \perp\!\!\!\perp Y_t \mid \mathbb{S}$ .
  - (c) Iteratively repeat step (b) while increasing the size of the conditioning set  $n$  by 1 until there are no more adjacent pairs  $(X_{t^*}, Y_t)$ , such that there is a subset  $\mathbb{S} \subseteq \mathbb{V}^* \setminus \{X_{t^*}, Y_t\}$  of size  $n$  that was not tested.
- CB2. Orient instantaneous relations using some rules (in case of causal sufficiency, see Spirtes et al., 2000, Meek, 1995).

Note that for step CB1 we only need Assumption 1, 2, 3, 5 and 6, while CB2 requires also faithfulness assumption, which is stronger than Assumptions 3. The output of the CB1 step is a partially oriented graph  $\hat{\mathcal{G}}^*$  that shares the same skeleton as the true graph  $\mathcal{G}^*$  and where all lagged relations are oriented and all instantaneous relations are non-oriented.

In our work, we consider two algorithms from this family. The first one, PCMC<sup>+</sup> (Runge, 2020), is an adaptation of the PC-algorithm to time series that can discover WCGs, and the second one, PCGCE (Assaad et al., 2022c), is an adaptation of the PC-algorithm that can discover ECGs.

## 4 Hybrids of constraint-based and noise-based algorithms

Here, we present a hybrid framework for discovering causal graphs from the observation of temporal data, which contains two classes of methods: noise-based-then-constraint-based (NBCB) and constraint-based-then-noise-based (CBNB). Both classes of methods have a common set of assumptions, such as standard Assumptions 1, 2, 5 related to the WCG (resp. ECG), Assumption 6 for stationary time series, and Assumption 4 for noise-based methods. As both classes use only part of the algorithms from the constraint-based family, they do not require the faithfulness assumption but only the weaker adjacency faithfulness, stated in Assumption 3. In the rest of the paper, we assume that methods from CBNB or NBCB classes are built using the algorithms from constraint-based and noise-based families that are correct under given assumptions.

Note that we do not need an acyclicity assumption of the true SCG graph, as in NBCB<sup>acyclic</sup>, as we start by inferring a WCG or an ECG and then can deduce the SCG from it.

In the following sections, we provide a detailed description of the NBCB and CBNB classes of methods.

### 4.1 NBCB class of algorithms

Each of the methods in NBCB class has two major steps. The first part of NBCB constructs a fully connected graph such that lagged relations are oriented using temporal priority, on which the NB1 step is applied in order to find the causal order between all instantaneous nodes.

In the second part, we aim to use CB1 to prune the edges. This step can be optimized by using additional information on the causal order. We modify CB1 step to CB1', by taking into account the causal order of the nodes in the following way:

<sup>2</sup>Note that Peters et al. (2014) considered the case where the minimality assumption is violated which is equivalent to the case where Assumption 3 is violated (Peters et al., 2017).

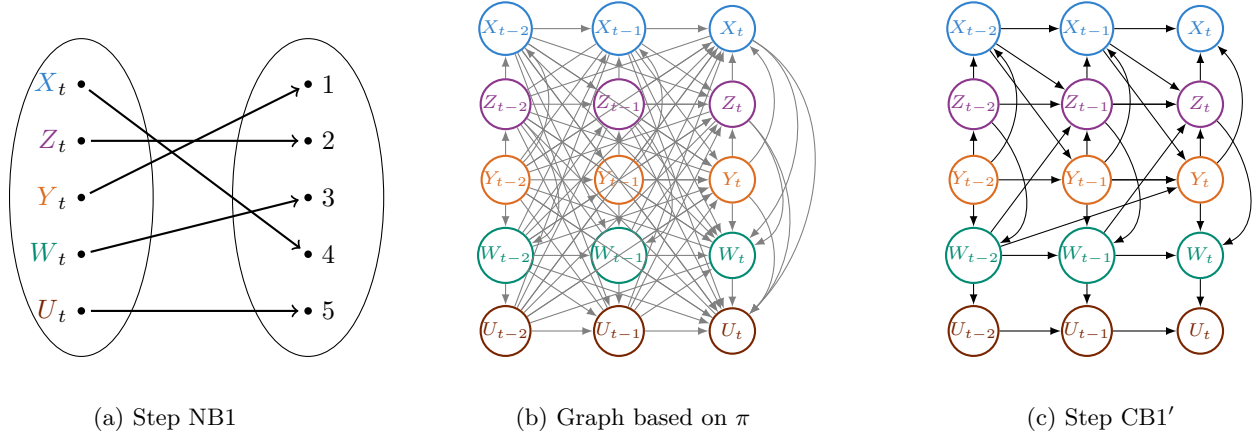


Figure 3: Illustration of the NBCB algorithm for the running example. (a) Output of the NB1 step (b) Output of the CB1'.

CB1'. Start with the initialization of the fully connected oriented graph as instantaneous relations can be oriented using the causal order  $\pi$ .

- (a) Eliminate edges between nodes<sup>3</sup>  $(X_{t^*}, Y_t)$  if  $X_{t^*} \perp\!\!\!\perp Y_t$ .
- (b) For each pair of nodes  $(X_{t^*}, Y_t)$  having an edge between them, and for each subset of nodes  $\mathbb{S} \subseteq \mathbb{V}^* \setminus \{X_{t^*}, Y_t\}$  of size  $n = 1$  such that  $\forall Z_{t'} \in \mathbb{S}, Z_{t'}$  is *parent* of  $Y_t$ , eliminate the edge between  $X_{t^*}$  and  $Y_t$  if  $X_{t^*} \perp\!\!\!\perp Y_t \mid \mathbb{S}$ .
- (c) Iteratively repeat step (b) while increasing the size of the conditioning set  $n$  by 1 until there are no more adjacent pairs  $(X_{t^*}, Y_t)$ , such that there is a subset  $\mathbb{S} \subseteq \mathbb{V}^* \setminus \{X_{t^*}, Y_t\}$  of size  $n$  that was not tested.

Note that in CB1' step (a) and (c) are the same as in step CB1. The NBCB class of methods can be presented as a combination of the NB1 and CB1', for which we provide a schematic illustration in Figure 3.

**Theorem 1.** Let  $\mathcal{G}^f = (\mathbb{V}^f, \mathbb{E}^f)$  be an FT CG. Under Assumptions 1, 2, 3, 4, 5, 6 and given perfect conditional independence information about all pairs of variables in  $\mathbb{V}^f$ , any algorithm in the NBCB class returns the correct WCG or the correct ECG compatible with  $\mathcal{G}^f$ .

The proof of Theorem 1 is available in Appendix A. It is important to note that after having obtained the WCG or the ECG, we can deduce the correct SCG using Definition 2.

The NBCB class is more robust to the violation of Assumption 3, compared to the original methods that were used for its construction. This means that even if Assumption 3 is violated, NBCB is still capable of providing valuable information on causal relationships, as demonstrated in the following proposition.

**Proposition 1** (Violation of Assumption 3). Under Assumptions 1, 2, 4, 5, 6 and given a correct causal order between instantaneous nodes, the NBCB class would give WCGs and ECGs such that, for each pair of nodes  $X_{t^*}$  and  $Y_t$ , one of the following possibilities holds true:

- (1) The causal relationship between  $X_{t^*}$  and  $Y_t$  is correctly identified.
- (2)  $X_{t^*}$  and  $Y_t$  are not adjacent in the inferred graph, but they are adjacent in the true graph.
- (3)  $X_{t^*}$  and  $Y_t$  are adjacent in the inferred graph, but they are not adjacent in the true graph.

The proof of Proposition 1 is presented in Appendix A. Proposition 1 states that if there is an oriented edge in a graph  $\hat{\mathcal{G}}^*$  inferred by NBCB, then it can not have an opposite orientation in the true graph. In the following, we illustrate cases (2) and (3) of the Proposition 1. Let us consider the true WCG  $\mathcal{G}^w$  in Figure 4a. As long as adjacency faithfulness is violated, we can assume that there exists a path  $\langle Z_{t-1}, X_{t-1}, X_t \rangle$  which is canceled

<sup>3</sup>We recall that  $t^*$  is a wildcard that represent time step  $t - i$ , where  $i \in \{0, \dots, \gamma\}$  in the context of WCG and represent either  $t-$  or  $t$  in context of ECG.



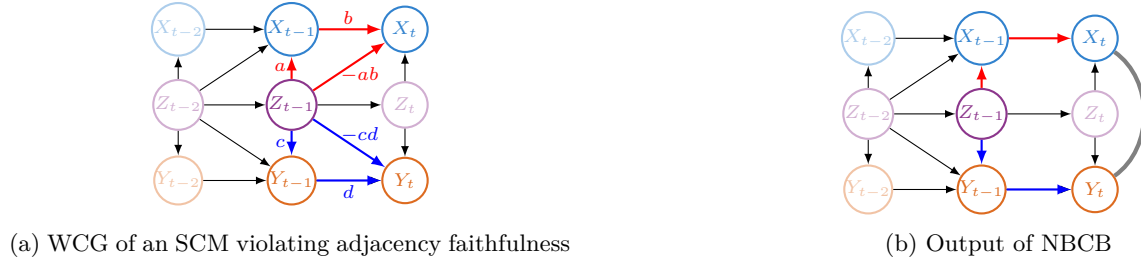


Figure 4: Illustration of items (2) and (3) in Proposition 1.

by path  $\langle Z_{t-1}, X_t \rangle$ , such that in the observed data  $Z_{t-1} \perp\!\!\!\perp X_t \mid \{X_{t-2}, Z_{t-2}\}$ , thus the edge  $Z_{t-1} - X_t$  would be removed, so we obtain case (2) in Proposition 1. A similar argument works for the edge  $Z_{t-1} - Y_t$ . Further, this error would propagate in the next step for the pair of nodes  $Y_t$  and  $X_t$ . As in the inferred graph  $\hat{\mathcal{G}}^w$ , edges  $Z_{t-1} - X_t$  and  $Z_{t-1} - Y_t$  are absent (see Figure 4b), then  $X_t \not\perp\!\!\!\perp Y_t \mid \text{Pa}_{\hat{\mathcal{G}}^w}(X_t) \cup \text{Pa}_{\hat{\mathcal{G}}^w}(Y_t)$ , as  $Z_{t-1}$  is the common confounder in the true graph, thus the edge  $X_t - Y_t$  would not be removed and we obtain the case (3) in Proposition 1.

We want to highlight that Proposition 1 holds when the CB1' step of NBCB is implemented using a PC-style algorithm. Other constraint-based algorithms could be envisioned, such as a greedy approach where the iterative process of finding conditional independence while progressively expanding the conditioning set (steps (b) and (c) of CB1') is replaced by a single step of conditioning on all parents. With such a greedy algorithm, the concerns outlined in case (3) of the proposition could be alleviated.

Note that NBCB would perform poorly when Assumption 4 is violated. In this case, NB1 would give an incorrect causal order, and the errors would propagate in the second step.

---

**Algorithm 1:** Noise-Based-then-Constraint-Based (NBCB)
 

---

**Input:** A multivariate time series, a maximal temporal lag  $\gamma$  and a significance threshold  $\alpha$ , NB1, CB1', an independence measure  $I()$ , and a conditional independence test  $CI()$

**Result:**  $\hat{\mathcal{G}}^*$  (WCG or ECG) and  $\hat{\mathcal{G}}^s$  (SCG)

Find the causal order  $\hat{\pi}$  between all instantaneous nodes using NB1 which takes  $\gamma$  and  $I()$  as hyper-parameters;

Discover  $\hat{\mathcal{G}}^*$  using CB1' which takes  $\gamma$ ,  $\alpha$ ,  $CI()$ , and  $\hat{\pi}$  as hyper-parameters;

Deduce the SCG  $\hat{\mathcal{G}}^s$  from  $\hat{\mathcal{G}}^*$  using Definition 2.

---

The pseudo-code of NBCB is given in Algorithm 1, which involves the abstract steps NB1 and CB1'. Step NB1 can be directly obtained from the existing algorithms. In the experimental section of this paper, step NB1 is directly based on the VarLiNGAM algorithm, while step CB1' is either based on the modification of the PCTMI<sup>+</sup> algorithm or on the modification of the PCGCE algorithm. More details on specific versions of NB1 and CB1' is given in Appendix B.

## 4.2 CBNB class of algorithms

As far as we know, there exists no previous work that investigated the case where the constraint-based part of a hybrid method is executed before the noise-based part in causal discovery from time series (for non-temporal data, see PClingam, Hoyer et al., 2008). In theory, there is no clear argument as to why one part should be executed before the other. So here, we present a new class of methods called CBNB, where the constraint-based part is before the noise-based part.

In the first step of CBNB, CB1 is used to infer  $\hat{\mathcal{G}}^*$ . Then, we are going to orient edges between instantaneous nodes  $V_t$  by finding the causal order between them.

A vanilla approach would be to apply NB1 over all instantaneous nodes (while taking into account lagged common confounders), as it was done in NBCB, to get the causal order and then orient the instantaneous relations accordingly. However, we argue that this vanilla approach, despite being correct, is not optimal since it does not take into account the knowledge that has already been acquired through the construction

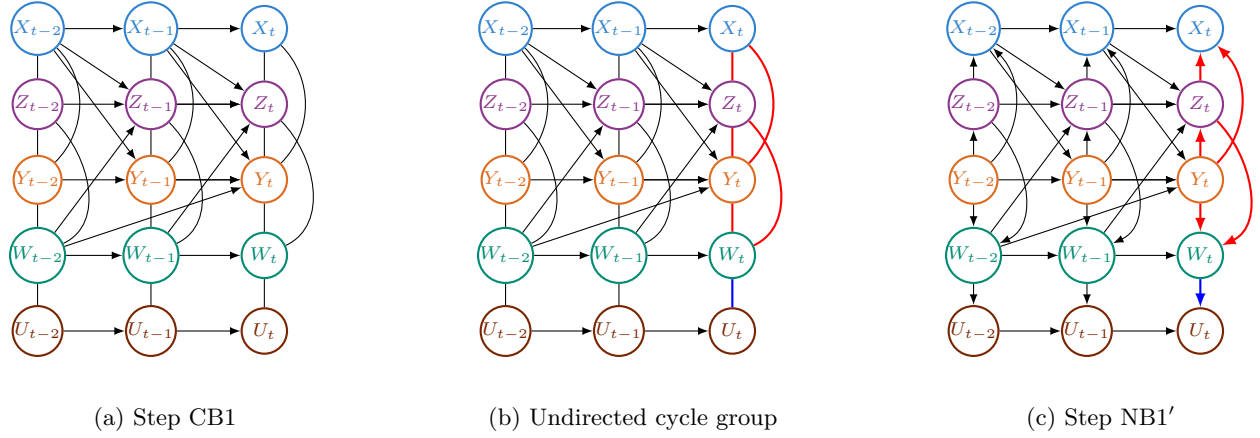


Figure 5: Illustration of the CBNB algorithm for the running example. (a) Output of the CB1 step (b) Detection of the undirected cycle group, where red and blue colours denote two different cycle groups of instantaneous nodes (c) Output of the NB1' on each of the cycle groups.

of the output graph in step CB1. Therefore, we modify the NB1 step to NB1' by finding the causal order within different groups of instantaneous nodes separately in the following way:

**NB1'.** Find the causal order between instantaneous groups of nodes  $\mathbb{I}_t \subseteq \mathbb{V}_t$  by recursively performing regression and independence tests between the predictors and residuals (noise). But note that even if only the instantaneous group of nodes  $\mathbb{I}_t$  are accounted for, the lagged parents  $Pa_{\hat{\mathcal{G}}^*}(\mathbb{I}_t) \setminus \mathbb{V}_t$  are used in the regression as a means to account for confounder bias.

Not any groups of instantaneous nodes  $\mathbb{I}_t$  would yield a correct causal order since, in general, for any  $X_t, Y_t \in \mathbb{I}_t$ ,  $\mathbb{I}_t \cup Pa_{\hat{\mathcal{G}}^*}(\mathbb{I}_t)$  does not necessarily contain any subset that remove confounding bias between  $X_t$  and  $Y_t$ . Therefore, these groups should be selected carefully. To find these groups, we first need to define an undirected cycle path.

We provide a schematic illustration in Figure 5 for the running example.

**Definition 5** (Undirected Cycle Path). Let  $\hat{\mathcal{G}}^*$  be the output of the CB1 step. A path  $\mathbf{u} = \langle X_t, Y_t, \dots, X_t \rangle$  is an undirected cycle path iff  $\mathbf{u}$  is an undirected path in  $\hat{\mathcal{G}}^*$  and only the first and last nodes of  $\mathbf{u}$  are equal, and  $\text{size}(\mathbf{u}) \geq 3$ .

For example, in Figure 5b there are undirected cycle paths between  $X_t, Y_t, Z_t$  and between  $Z_t, Y_t, W_t$ , so  $Z_t - Y_t$  would be in both cycles and would be considered twice, which is not only a computational problem but might also induce bias in practice. Thus, defining a cycle path alone is not sufficient. So, we combine all cycle paths that share at least one edge in a cycle group<sup>4</sup> which is defined as follows:

**Definition 6** (Undirected Cycle Group). Let  $\hat{\mathcal{G}}^*$  be the output of the CB1 step.  $\mathbb{C}$  is an undirected cycle group of  $\hat{\mathcal{G}}^*$  iff  $\mathbb{C}$  is a set of undirected cycle paths and  $\forall \mathbf{u}_1, \mathbf{u}_2 \in \mathbb{C}, \mathbf{u}_1 \cap \mathbf{u}_2 \neq \emptyset$ .

Given an undirected cycle group  $\mathbb{C}$ , we say that a node  $X_t$  belongs to  $\mathbb{C}$  iff  $\exists \mathbf{u} \in \mathbb{C}$  such that  $X_t \in \mathbf{u}$  and we say that an edge  $X_t - Y_{t'}$  belongs to  $\mathbb{C}$  iff  $\exists \mathbf{u} \in \mathbb{C}$  such that  $\langle X_t, Y_{t'} \rangle \in \mathbf{u}$ . In Figure 5b there are two undirected cycle groups, the first contains nodes  $X_t, Y_t, Z_t, W_t$  and the second contains nodes  $U_t, W_t$ . Here we provide an example for the WCG, but the same applies to the corresponding ECG.

Having brought out the concept of undirected cycle group, we can now describe the second (noise-based) part of CBNB. Given the output of the CB1 step, CBNB searches for all undirected cyclic groups. Then for each undirected cyclic group  $\mathbb{C}$ , CBNB uses NB1' to find the causal order  $\pi$  between all the nodes belonging to undirected cyclic group  $\mathbb{C}$ . Finally, using this causal order, CBNB orient all edges belonging to  $\mathbb{C}$ .

Note that the CBNB step where NB1' is applied for different undirected cycle groups can be parallelized, which can significantly improve the computational time for high dimensional problems.

<sup>4</sup>Note that our definition of cycle group is different than the one introduced in [Spirtes \(1995\)](#).

**Theorem 2.** Let  $\mathcal{G}^f = (\mathbb{V}^f, \mathbb{E}^f)$  be an FTCTG. Under Assumptions 1, 2, 3, 4, 5, 6 and given perfect conditional independence information about all pairs of variables in  $\mathbb{V}^f$ , any algorithm in the CBNB class returns the correct WCG or the correct ECG compatible with  $\mathcal{G}^f$ .

The proof of Theorem 2 is available in Appendix A. It is also important to note that as in the case of NBCB, after having obtained the WCG or the ECG, we can deduce the correct SCG using Definition 2.

**Proposition 2** (Violation of Assumption 4). Under Assumptions 1, 2, 3, 5, 6 and given perfect conditional independence information about all pairs of variables, CBNB is guaranteed to find the correct skeleton of the WCG or the ECG.

The proof of Proposition 2 is available in Appendix A. Note that since CBNB gives the correct skeleton of WCGs and ECGs, the correct skeleton of SCG can also be deduced. If Assumption 3 is violated, then the skeleton obtained in the CB1 step of CBNB is not reliable, thereby affecting the reliability of the CBNB algorithm’s results.

The pseudo-code of CBNB is given in Algorithm 2, which involves the abstract steps CB1 and NB1’. In the experimental section of this paper, step CB1 is directly based either on the PCMCi<sup>+</sup> algorithm or on the PCGCE algorithm, while step NB1’ is based on the modification of the VarLiNGAM algorithm. More details on specific versions of CB1 and NB1’ is given in Appendix B.

---

**Algorithm 2:** Constraint-Based-then-Noise-Based (CBNB)

---

**Input:** A multivariate time series, a maximal temporal lag  $\gamma$  and a significance threshold  $\alpha$ , CB1, NB1’, an independence measure  $I()$ , and a conditional independence test  $CI()$

**Result:**  $\hat{\mathcal{G}}^*$  (WCG or ECG) and  $\hat{\mathcal{G}}^s$  (SCG)

Initialize  $\hat{\mathcal{G}}^*$  as the output of CB1 which takes  $\gamma$ ,  $\alpha$ , and  $CI()$  as hyper-parameters;

**for** each undirected cycle group  $\mathbb{C}$  in  $\hat{\mathcal{G}}^*$  **do**

$\mathbb{I}_t$ : set of nodes that belong to  $\mathbb{C}$ ;

    Find the causal order  $\hat{\pi}$  between nodes in  $\mathbb{I}_t$  using NB1’ which takes  $\gamma$ ,  $I()$ , and  $\hat{\mathcal{G}}^*$  as hyper-parameters;

    Orient instantaneous edges between  $\mathbb{I}_t$  in  $\hat{\mathcal{G}}^*$  using the order  $\hat{\pi}$ ;

Deduce the SCG  $\hat{\mathcal{G}}^s$  from  $\hat{\mathcal{G}}^*$  using Definition 2

---

## 5 Experiments

In this section, we propose first an extensive analysis<sup>5</sup> both on simulated data, generated from basic causal structures, and on simulated but realistic benchmarks. We then perform an analysis on different real datasets.

### 5.1 Experimental setup

**Baselines and hyper-parameters.** We compare NBCB and CBNB with five state-of-the-art methods:

- the multivariate version of Granger Causality denoted GCMVL (Arnold et al., 2007);
- the constraint-based methods PCMCi<sup>+</sup> (Runge, 2020) for which we use the Python code available at <https://github.com/jakobrunge/tigramite> and PCGCE (Assaad et al., 2022c) for which the main Python code available at <https://github.com/ckassad/PCGCE>. For PCGCE, as the authors suggested, we reduce the dimensionality of  $\mathbb{V}_{t-}$  in the ECG to 1 using PCA;
- the score-based method Dynotears (Pamfil et al., 2020), for which the Python code is available at <https://github.com/quantumblacklabs/causalnex>. For this method, we set the hyperparameters to their recommended values ( $\lambda_W = \lambda_A = 0.05$  and  $\alpha_W = \alpha_A = 0.01$ );
- the noise-based method VarLiNGAM (Hyvärinen et al., 2008) for which we use the Python code available at <https://github.com/cdt15/lingam> where the regularization parameter in the adaptive Lasso is selected using BIC.

---

<sup>5</sup>The code of all our methods and of every experimentation is available in Supplementary Materials and will be rendered available online if the paper will be accepted.

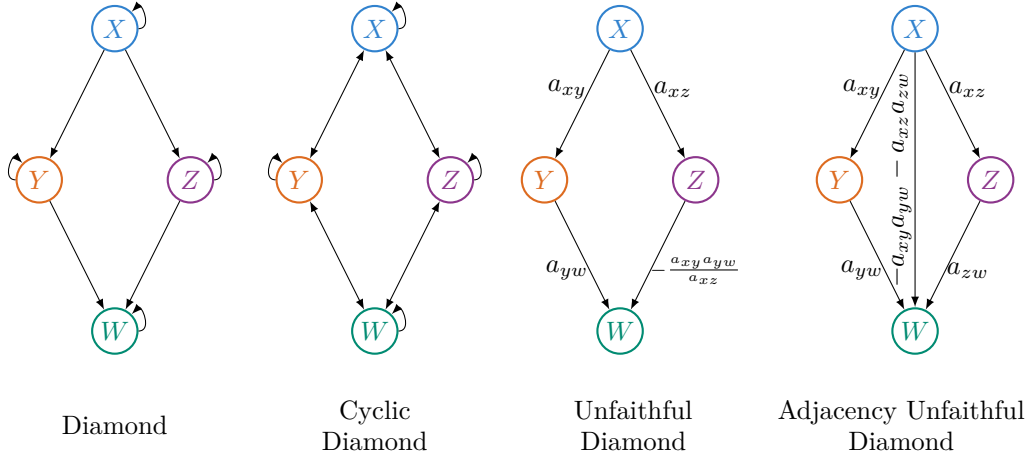


Figure 6: Summary causal graphs corresponding to the data simulated in Section 5.2. The last two models correspond to an unfaithful distribution.

For all the methods, the maximal temporal lag is set to  $\gamma = 5$  and the significant threshold for hypothesis testing to  $\alpha = 0.05$ . We test two versions of each of our classes which we denote NBCB-w, NBCB-e, CBNB-w, and CBNB-e. In NBCB-w and NBCB-e, the NB1 step is based on the VarLiNGAM algorithm and the CB1' step is respectively based on the PCMCi<sup>+</sup> algorithm and the PCGCE algorithm. In CBNB-w and CBNB-e, the CB1 step is respectively based on the PCMCi<sup>+</sup> algorithm and the PCGCE algorithm and the NB1' step is based on the VarLiNGAM algorithm. The pseudo-code of each version of the NB1, CB1, NB1', CB1' steps are given in Appendix B. To find undirected cycle paths in CBNB-w and CBNB-e we use an adapted version of Paton's algorithm (Paton, 1969). For all methods that require a conditional independence test, we use a test based on partial correlation, which assumes Gaussian distributions but which has been successfully used on non-iid data (Peters et al., 2013).

**Evaluation.** In the different experimental settings, we compared the results concerning the F1 score of the orientations in the SCG obtained without considering self causes, as it is treated differently depending on the methods. When there are three datasets or more, we report the mean and standard deviation for the F1 score.

## 5.2 Simulated data with Gaussian and non-Gaussian noise

The simulated datasets correspond to four causally sufficient SCGs presented in Figure 6, extracted from WCGs  $\mathcal{G}^w$ , among which three are acyclic, two correspond to an unfaithful distribution, and one is cyclic. The generating process of all datasets is the following: for all  $Y$ , for all  $t > 0$ ,

$$Y_t = a_y Y_{t-1} + \sum_{X_{t-\ell} \in \text{Pa}_{\mathcal{G}^w}(Y_t, \mathcal{G}^w)} a_{xy} X_{t-\ell} + 0.1 \xi_t^y,$$

where  $a_y, a_{xy} \in U([-1, -0.1] \cup [0.1, 1])$  and for each parent  $X$  we randomly choose if  $X$  causes  $Y$  instantaneously or with a lag of 1, i.e.,  $\ell \in \{0, 1\}$ . Regarding the noise, we consider two different settings, in the first the noise is drawn from a uniform distribution, i.e.,  $\xi^y \sim U([-1, 1])$ , and in the second the noise is drawn from a Gaussian distribution, i.e.,  $\xi^y \sim N(0, 1)$ . For each setting and each structure in Figure 6 we generate 100 datasets of 1000 timestamps.

For the unfaithful diamond structure in Figure 6, following Zhalama et al. (2016), we set  $a_y$  as zero, and  $a^{yw} = -a^{xz}a^{zw}/a^{xy}$ . All relationships are considered instantaneous. Consequently, in the distribution consistent with this model, we observe  $X \perp\!\!\!\perp W$ , which violates the faithfulness assumption as this independence is not entailed by the causal Markov condition. However, it does not violate the adjacency faithfulness assumption since  $X$  is not adjacent to  $W$  in the graph. Similarly, for the adjacency unfaithful diamond structure, we set  $a^{yw} = -a^{xy}a^{yw} - a^{xz}a^{zw}$ , which violates the adjacency faithfulness assumption since in addition to  $X$  being adjacent to  $Y$  in the graph, in the distribution, we observe  $X \perp\!\!\!\perp W$ , and this independence is not entailed by the causal Markov condition.

Table 1: Results obtained on the simulated data of Section 5.2 for the different structures with 1000 observations with non-Gaussian noise (top panel) and with Gaussian noise (bottom panel). We report the mean and the standard deviation of the F1 score of the orientations in the SCG. The best results are in blue bold and the second best results are in green bold.

	Diamond	Cyclic Diamond	Unf. Diamond	Adj. unf. Diamond
Non-Gaussian noise				
NBCB-w	<b>0.94</b> $\pm$ 0.01	<b>0.81</b> $\pm$ 0.01	0.86 $\pm$ 0.01	0.8 $\pm$ 0.01
CBNB-w	<b>0.94</b> $\pm$ 0.01	<b>0.8</b> $\pm$ 0.01	0.9 $\pm$ 0.01	0.84 $\pm$ 0.01
NBCB-e	0.74 $\pm$ 0.02	0.72 $\pm$ 0.01	0.95 $\pm$ 0.01	<b>0.86</b> $\pm$ 0.01
CBNB-e	0.74 $\pm$ 0.02	0.7 $\pm$ 0.02	<b>0.96</b> $\pm$ 0.01	<b>0.86</b> $\pm$ 0.01
GCMVL	0.86 $\pm$ 0.01	0.68 $\pm$ 0.01	0.04 $\pm$ 0.01	0.04 $\pm$ 0.01
PCMCI <sup>+</sup>	0.92 $\pm$ 0.01	0.75 $\pm$ 0.01	0.47 $\pm$ 0.04	0.44 $\pm$ 0.03
PCCGE	0.69 $\pm$ 0.02	0.66 $\pm$ 0.01	0.5 $\pm$ 0.01	0.45 $\pm$ 0.01
Dynotears	0.03 $\pm$ 0.01	0.0 $\pm$ 0.0	0.0 $\pm$ 0.0	0.0 $\pm$ 0.0
VarLiNGAM	<b>0.99</b> $\pm$ 0.01	0.79 $\pm$ 0.01	<b>0.98</b> $\pm$ 0.01	<b>0.87</b> $\pm$ 0.01
Gaussian noise				
NBCB-w	0.78 $\pm$ 0.03	<b>0.77</b> $\pm$ 0.01	<b>0.52</b> $\pm$ 0.05	<b>0.48</b> $\pm$ 0.01
CBNB-w	0.8 $\pm$ 0.04	<b>0.75</b> $\pm$ 0.01	<b>0.52</b> $\pm$ 0.05	<b>0.48</b> $\pm$ 0.06
NBCB-e	0.64 $\pm$ 0.02	0.67 $\pm$ 0.02	<b>0.52</b> $\pm$ 0.07	<b>0.44</b> $\pm$ 0.06
CBNB-e	0.72 $\pm$ 0.03	0.65 $\pm$ 0.02	<b>0.53</b> $\pm$ 0.07	<b>0.44</b> $\pm$ 0.05
GCMVL	<b>0.87</b> $\pm$ 0.01	0.7 $\pm$ 0.01	0.03 $\pm$ 0.01	0.01 $\pm$ 0.01
PCMCI <sup>+</sup>	<b>0.93</b> $\pm$ 0.01	<b>0.75</b> $\pm$ 0.01	0.42 $\pm$ 0.05	0.4 $\pm$ 0.04
PCCGE	0.69 $\pm$ 0.02	0.65 $\pm$ 0.01	0.5 $\pm$ 0.02	<b>0.44</b> $\pm$ 0.01
Dynotears	0.06 $\pm$ 0.02	0.0 $\pm$ 0.0	0.0 $\pm$ 0.0	0.0 $\pm$ 0.0
VarLiNGAM	0.78 $\pm$ 0.03	0.74 $\pm$ 0.01	0.5 $\pm$ 0.07	0.42 $\pm$ 0.06

In Table 1, we report the results for the setting with non-Gaussian noise (top panel), and with Gaussian noise (bottom panel). In the case of non-Gaussian noise, for the first two structures, diamond and cyclic diamond all assumptions required by both families of methods are satisfied. In this case, VarLiNGAM has the best performance for diamond, followed by CBNB-w and NBCB-w, while CBNB-w and NBCB-w have the best performance for cyclic diamond, followed by VarLiNGAM. The closest to these methods is PCMCI<sup>+</sup>. From these results, we can see that CBNB-w and NBCB-w perform better than both original noise-based and constraint-based methods or as a trade-off between them. We can note that the same conclusion can be made for NBCB-e and CBNB-e.

For the unfaithful structures, where the constraint-based methods PCMCI<sup>+</sup> and PCCGE have a drop in performance due to faithfulness violation, VarLiNGAM has the best results, followed by CBNB-e, with close results by NBCB-e. Except NBCB-e and CBNB-w, all other methods have significantly lower performance. We can also note that our methods experience a noticeable drop in performance only for adjacency unfaithful structures, confirming that they do not require full faithfulness assumption.

In the case of Gaussian noise, we can note the drop in performance of VarLiNGAM due to violation of Assumption 4 for the first diamond structure, PCMCI<sup>+</sup> performs best, closely followed by GCMVL and CBNB-w, NBCB-w and VarLiNGAM. For cyclic diamond structure, NBCB-w has the best results, followed by CBNB-w and PCMCI<sup>+</sup>. For unfaithful structures with Gaussian noise, our methods have the best results. Specifically, CBNB-e performs best for the unfaithful diamond, with the rest of our methods being second best. NBCB-w and CBNB-w work best for the adjacency unfaithful diamond, followed by NBCB-e, CBNB-e algorithms and PCCGE. We can see from Gaussian noise simulation results, that when the assumptions for constraint-based methods are satisfied, our methods (CBNB-w and NBCB-w) are either trade-offs between the PCMCI<sup>+</sup> and VarLiNGAM or perform better. On the other hand in most cases, NBCB-e and CBNB-e, are trade-offs between PCCGE and VarLiNGAM. For the unfaithful structures under assumption violation, all our methods are more robust compared to constraint and noise-based families.



Table 2: Results for realistic datasets of Section 5.3 generated using the Lotka–Volterra model with five species (left column) and ten species (right column). We report the mean and the standard deviation of the F1 score of the orientations in the SCG. The best results are in blue bold and the second best results are in bold green.

	Lotka–Volterra(5)	Lotka–Volterra(10)
NBCB-w	<b>0.40</b> $\pm$ 0.03	<b>0.26</b> $\pm$ 0.01
CBNB-w	0.34 $\pm$ 0.04	<b>0.24</b> $\pm$ 0.01
NBCB-e	<b>0.40</b> $\pm$ 0.02	0.19 $\pm$ 0.01
CBNB-e	<b>0.36</b> $\pm$ 0.03	0.21 $\pm$ 0.01
GCMVL	0.21 $\pm$ 0.03	0.13 $\pm$ 0.01
PCMCI <sup>+</sup>	0.33 $\pm$ 0.04	0.21 $\pm$ 0.01
PCGCE	<b>0.36</b> $\pm$ 0.03	0.2 $\pm$ 0.01
Dynotears	0.0 $\pm$ 0.0	0.0 $\pm$ 0.0
VarLiNGAM	0.22 $\pm$ 0.06	0.22 $\pm$ 0.02

Finally, comparing PCMCI<sup>+</sup> and PCGCE we can see that PCGCE has lower performance in general, except for the unfaithful cases for both types of noise distribution. This empirical observation suggests that PCGCE is more robust to assumption violation. This behaviour is also inherited by CBNB-e and NBCB-e methods. Table 1 presents the F1 score of the orientations in the SCG, which is not suitable to illustrate the Proposition 2. Thus, in Table 5 in Appendix E we present the F1 score on the adjacencies, which illustrate the robustness of CBNB class to Assumption 4. More precisely, CBNB-w has the same performance as PCMCI<sup>+</sup> and better than the results of NBCB-w, in the case of Gaussian noise, for all structures, except the adjacency unfaithful diamond. We also see similar results for CBNB-e. Proposition 1 is difficult to see from Table 1, as we do not evaluate separately orientations and adjacencies, due to the specific structure of the inferred graph.

### 5.3 Realistic ecological data from the Lotka–Volterra model

We consider the simulation with multi-species generalization of the Ricker model introduced by Poggiato et al. (2022), which is analogous to the generalized Lotka–Volterra model with abiotic control presented in the same paper and is commonly used in ecological studies. Ricker model with abiotic control in discrete time for abundance of species  $Y$  at time step  $t$  has the following form:

$$Y_t = \begin{cases} Y_{t-1} \exp \left( \Delta t \left( \sum_{X_{t-1} \in \text{Pa}_{\mathcal{G}^w}(Y_t, G^w)} a_{xy} X_{t-1} + \bar{Y} (-a_y) \exp \left( -\frac{(o_y - x)^2}{2\sigma_y^2} \right) \right) + \xi_t^y \right), & (\text{preys}) \\ Y_{t-1} \exp \left( \Delta t \left( \sum_{X_{t-1} \in \text{Pa}_{\mathcal{G}^w}(Y_t, G^w)} a_{xy} X_{t-1} - \mu \right) + \xi_t^y \right), & (\text{predators}) \end{cases}$$

where  $Y_t$  is the abundance of species  $Y$  at time  $t$ , the upper equation is related to preys and the lower to predator species,  $\bar{Y}$  is the abundance of species  $Y$  in the stationary state,  $a_{xy}$  is the strength of the effect of species  $X$  on species  $Y$  and  $a_y$  is strength of the effect of species  $Y$  on itself,  $\xi_t^y$  is an i.i.d Gaussian random variable with variance  $\sigma_r$ ,  $o_y$  is a niche optimum for species  $Y$ ,  $x$  is the environmental variable,  $\mu$  is the extinction rate of the predator. We run this simulation for the number of species  $S = \{5, 10\}$  with the following fixed parameters: fixed environment  $x = 0.5$ , number of time steps  $T = 1000$ ,  $\mu = 0.05$ ,  $\sigma_r = 0.2$  randomly assign  $o_y$  for each species between 0 and 1, the interaction matrix related to coefficients  $a_{xy}$  and  $a_y$  is obtained through randomly generated graph  $\mathcal{G}$ , such that  $\mathcal{G}$  has 3 trophic levels and  $\mathcal{G}$  is connected graph (for more details see Poggiato et al., 2022). All links in this graph are bi-directed, and the interaction strength is randomly sampled for all interactions. We generate 100 graphs and thus we obtain 100 datasets. On these datasets, NBCB-w performs better than the other methods followed by NBCB-e as shown in Table 2. Close to them perform CBNB-e, CBNB-w and PCGCE. Dynotears has the lowest result.

Table 3: Results for real datasets of Section 5.4. We report the mean and the standard deviation (when meaningful, see data description) of the F1 score of the orientations in the SCG. The best results are in blue bold and the second best results are in green bold.

	Temp.	Veil1	Veil2	Dairy	Ingest.	Web1	Web2	Antivirus1	Antivirus2
NBCB-w	<b>1</b>	<b>1</b>	0	<b>0.4</b>	$0.47 \pm 0.03$	0.2	0.23	0.13	0.3
CBNB-w	<b>1</b>	<b>1</b>	0	<b>0.4</b>	$0.46 \pm 0.11$	<b>0.24</b>	0.29	0.18	0.18
NBCB-e	<b>1</b>	<b>1</b>	<b>1</b>	<b>0.4</b>	$0.5 \pm 0.05$	<b>0.24</b>	<b>0.42</b>	<b>0.29</b>	<b>0.38</b>
CBNB-e	<b>1</b>	<b>1</b>	<b>1</b>	<b>0.4</b>	<b>0.52</b> $\pm 0.06$	0.15	<b>0.38</b>	<b>0.33</b>	0.27
GCMVL	0.67	<b>1</b>	<b>1</b>	0.33	$0.5 \pm 0.03$	0.19	0.0	0.08	0.0
PCMCI <sup>+</sup>	<b>1</b>	<b>1</b>	0	<b>0.4</b>	$0.3 \pm 0.08$	0.17	0.32	0.04	0.11
PCGCE	<b>1</b>	<b>1</b>	<b>1</b>	<b>0.4</b>	<b>0.55</b> $\pm 0.03$	0.21	0.34	<b>0.29</b>	<b>0.36</b>
Dynotears	0.67	<b>1</b>	<b>1</b>	0.33	$0.25 \pm 0.06$	0.22	0.3	0.18	0.17
VarLiNGAM	<b>1</b>	<b>1</b>	<b>1</b>	<b>0.5</b>	$0.49 \pm 0.05$	<b>0.23</b>	0.2	0.18	0.18

## 5.4 Real data

Nine different real datasets are considered in this study. We detail the performance of each method in the following paragraphs, while the results<sup>6</sup> are summarized in Table 3. See Appendix D for URL links to the considered datasets.

**Temperature.** This is a bivariate time series of length 168 about indoor  $I$  and outdoor  $O$  measurements. As noted by Assaad et al. (2021), it is expected that  $O$  causes  $I$ . NBCB-w, CBNB-w, NBCB-e, CBNB-e, PCMCI<sup>+</sup>, PCGCE, and VarLiNGAM correctly infer  $O \rightarrow I$ . GCMVL and Dynotears infer a bidirected causal relation.

**Veilleux.** We considered two datasets for Figure 11(a) and 12(a) (Jost & Ellner, 2000) from Veilleux (1979) which study interactions between predatory ciliate *Didinium nasutum* and its prey *Paramecium aurelia* with different values of Cerophyl concentrations (CC): 0.375 and 0.5. The lengths of the time series are 71 and 65. These data were previously analyzed with causal discovery algorithms (Barraquand et al., 2021, Sugihara et al., 2012), which showed bidirectional relationships in both cases.

Here, NBCB-e, CBNB-e, GCMVL, PCGCE, Dynotears and VarLiNGAM discover bidirected relationships *Paramecium*  $\leftrightarrow$  *Didinium* in both datasets, which is consistent with Sugihara et al. (2012), Barraquand et al. (2021). CBNB-w, NBCB-w, PCMCI<sup>+</sup> have detected bidirected relationships between *Paramecium* and *Didinium* only in the first dataset.

**Diary.** This dataset provides ten years (from 09/2008 to 12/2018) of monthly prices for milk  $M$ , butter  $B$ , and cheddar cheese  $C$ , so the three time series are of length 124. We expect that the price of milk is a common cause of the price of butter and the price of cheddar cheese:  $B \leftarrow M \rightarrow C$ .

NBCB-w, CBNB-w, NBCB-e, CBNB-e, PCMCI<sup>+</sup>, PCGCE and VarLiNGAM correctly inferred that  $M \rightarrow B$ . But NBCB-w and CBNB-w wrongly inferred that  $M \leftarrow C \rightarrow B$ , NBCB-e, CBNB-e, wrongly inferred that  $M \leftarrow B \leftarrow C$ , PCMCI<sup>+</sup> and PCGCE wrongly inferred that  $M \leftarrow C \leftarrow B$  and VarLiNGAM wrongly inferred that  $C \rightarrow B$ . GCMVL wrongly infers  $B \leftrightarrow M \leftarrow C \rightarrow B$  and Dynotears wrongly infers  $M \leftrightarrow B \leftrightarrow C$ .

**Ingestion mini.** This benchmark provided by EasyVista consists of 24 datasets each containing three time series with 1000 timestamps collected from an IT monitoring system with a one-minute sampling rate. Half the datasets are compatible with the graph  $C.M.I \leftarrow M.E \rightarrow G.H.I$  (Assaad et al., 2022b) where  $M.E$  is the metric extraction which represents the activity of the extraction of the metrics from the messages;  $G.H.I$  is the group history insertion, which represents the activity of the insertion of the historical status in the database; and  $C.M.I$  is the collector monitoring information, which represents the activity of the updates in a given database. The second half of the datasets are compatible with the graph  $M.D \rightarrow M.E \rightarrow M.I$  where  $M.D$  is the metric dispatcher which represents the activity of a process that orients messages to other processes with respect to different types of messages; and  $M.I$  is the metric insertion which represents the

<sup>6</sup>The results we obtained for VarLiNGAM on the temperature and the Dairy datasets are different than the results reported in Assaad et al. (2021) and we confirm with the authors that results we obtained are correct.

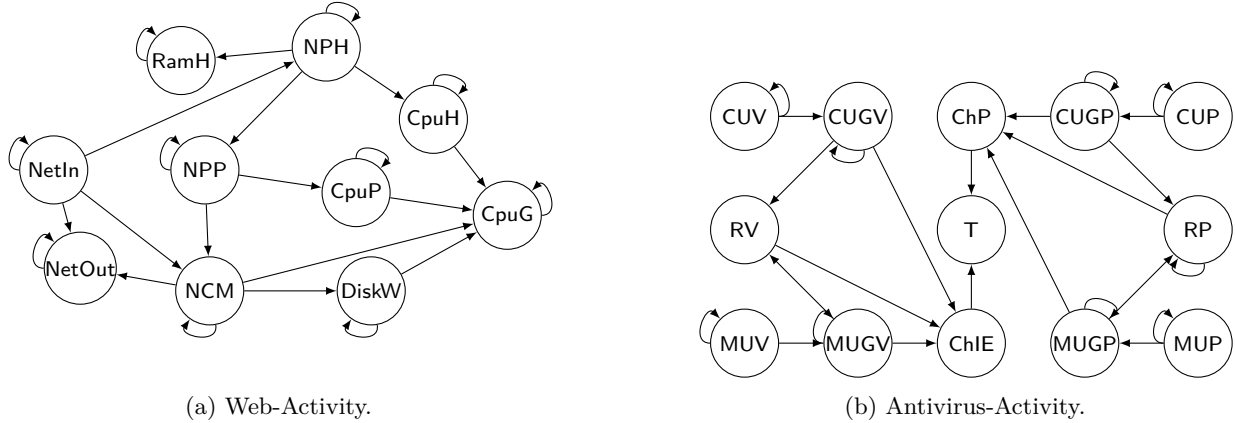


Figure 7: Summary causal graphs for (a) the Web activity datasets and (b) the Antivirus activity datasets. Those summary causal graphs are constructed by an IT monitoring system’s experts.

activity of insertion of data in a database. Lags between time series are unknown, as well as the existence of self-causes.

From Table 3, we can see that PCGCE has the best results followed by CBNB-e then by NBCB-e and GCMVL. After that comes VarLiNGAM and NBCB-w and CBNB-w and PCMCI<sup>+</sup>.

Finally, Dynotears has the worst result. This might suggest that the lags between causes and effects are not consistent over time, in the sense that if the lags between two-time series vary (while respecting the maximal temporal lag), the extended summary causal graph might remain the same however this is not true for the window causal graph. In this case, we might expect that methods inferring window causal graphs (such as PCMCI<sup>+</sup>) would perform worse than methods inferring extended summary causal graphs (such as PCGCE).

**Web.** We consider a dataset that reflects the activity in a web server which is provided by EasyVista. This dataset contains ten time series collected with a one-minute sampling rate. The raw data of this case study were initially misaligned. In order to align them, we use the two pre-processing strategies described in Appendix C. We denote the dataset pre-processed using Strategy 1 as Web 1 and the dataset pre-processed using Strategy 2 as Web 2. The two processed datasets contain 3000 timestamps. The corresponding summary causal graph for Web dataset is presented in Figure 7a where *NetIn* represents the data received by the network interface card in Kbytes/second; *NetOut* represents the data transmitted out by the network interface card in Kbytes/second; *NPH* represents the number of HTTP processes; *NPP* represents the number of PHP processes; *NCM* represents the number of open MySQL connections which are started by PHP processes; *CpuH* represents the percentage of CPU used by all HTTP processes; *RamH* represents the percentage of RAM used by all HTTP processes; *CpuP* represents the percentage of CPU used by all PHP processes; *DiskW* represents the Disk write in Kbytes/second; *CpuG* represents the percentage of global CPU usage.

From Table 3, for the Web1 dataset, we can see that NBCB-e and CBNB-w demonstrate the highest performance, followed by VarLiNGAM. Next are Dynotears and PCGCE. CBNB-e exhibits the lowest score. For the Web2 dataset, NBCB-e attains the highest F1 score, with CBNB-e closely following. The subsequent competitive results are observed with PCGCE and PCMCI<sup>+</sup>. This could imply that the data is noisy and the time lags are inconsistent throughout time, making the inference of the extended summary graph more robust.

**Antivirus.** Lastly, we consider a dataset which depicts the impacts of antivirus activity in servers which is again provided by EasyVista. This dataset contains 13 time series such that 3 of them are collected with a one-minute sampling rate and the rest with a five-minute sampling rate. The raw data of this case study were initially misaligned. To align them, we use the two pre-processing strategies described in Appendix C, leading to the dataset Antivirus 1 for Strategy 1 and Antivirus 2 for Strategy 2. The two processed datasets consist of 1321 timestamps. The corresponding summary causal graph for Antivirus dataset is presented in Figure 7b where *CUV* represents the percentage of CPU usage of antivirus processes in server V; *CUGV*

represents the percentage of CPU usage of the global server V;  $MUV$  represents the percentage of memory usage of antivirus process;  $MUGV$  represents the percentage of global memory usage of the server;  $RV$  represents the Disk IO read in Kbytes/second;  $ChIE$  refers to the required duration in seconds to open an *IE browser* on server V;  $CUP$  represents the percentage of CPU usage of antivirus processes in server P;  $CUGP$  represents the percentage of CPU usage of the global server P;  $MUP$  represents the percentage of memory usage of antivirus process;  $MUGP$  represents the percentage of global memory usage of the server;  $RP$  represents the Disk IO read in Kbytes/second;  $ChP$  represents refers to the required duration in seconds to open a *CITRIX Portal* on server P;  $T$  represents the global time in seconds required to open a CITRIX portal and open the IE browser.

From Table 3 for Antivirus 1, we can see that CBNB-e achieves the best result followed by PCGCE and NBCB-e and then by CBNB-w, VarLiNGAM and Dynotears. GCMVL and PCMCI<sup>+</sup> have low performance, with PCMCI<sup>+</sup> being the worst. For Antivirus 2, we can see that NBCB-e performs best followed by PCGCE and then by CBNB-e. The remaining methods have a substantial drop in performance. As in the case of Web datasets, improved performance of the PCGCE over PCMCI<sup>+</sup> suggests that inference of the extended summary graph is more robust in this case. We can also note that NBCB-e and NBCB-w perform well, while VarLiNGAM does not, which could suggest that VarLiNGAM infers a more dense graph.

## 6 Discussion

Experiments on simulated data, realistic ecological data, and real data from various applications, show that our hybrid approaches are robust and yield overall good results over all datasets. Notice that for all results on real data, NBCB-w and CBNB-w (which are based on PCMCI<sup>+</sup> and VarLiNGAM) never perform simultaneously worse than PCMCI<sup>+</sup> and VarLiNGAM. Similarly, NBCB-e and CBNB-e (which are based on PCGCE and VarLiNGAM) never perform simultaneously worse than PCGCE and VarLiNGAM, except for the Web 1 dataset where CBNB-e has the lowest F1-score (but NBCB-e has the best F1-score). In general, NBCB-e and CBNB-e seem to be more reliable than NBCB-w and CBNB-w for the real data we considered. As mentioned before, the possible explanation is noisy data and inconsistent time lags.

Class	NBCB		CBNB	
Version	NBCB-e	NBCB-w	CBNB-e	CBNB-w
Output	ECG	WCG	ECG	WCG
Step 1	NB1 (VLiNGAM)		CB1 (PCGCE - PCMCI <sup>+</sup> )	
Step 2	CB1' (PCGCE - PCMCI <sup>+</sup> )		NB1' (VLiNGAM)	
Violation of Assump. 3	$(X \rightarrow Y \in \hat{\mathcal{G}}) \Rightarrow (Y \not\rightarrow X \in \mathcal{G})$		✗	✗
Violation of Assump. 4	✗	✗	$(X - Y \in \hat{\mathcal{G}}) \Rightarrow (X - Y \in \mathcal{G})$	
Simulated data (Sec. 5.2)	✗	✓	✗	✓
Realistic sim. data (Sec. 5.3)	✓	✓	✓	✓
Real data (Sec. 5.4)	✓	✗	✓	✗

Table 4: Summary of the two proposed classes of methods, NBCB and CBNB. Rows respectively indicate: their versions NBCB-e, NBCB-w, CBNB-e, CBNB-w; outputs; the algorithms used in each step; their theoretical guarantees, or lack thereof (✗), under violation of some assumption; and their advantageous (✓) or limited (✗) performances on the different data scenarios considered in Section 5.

In summary, results on simulated data, realistic ecological data, and real data are coherent with the theoretical findings, showing that algorithms from CBNB and NBCB classes are trade-offs between the original methods, potentially exhibiting enhanced performance compared to the original methods when certain assumptions are violated. In Table 4, we provide various theoretical and experimental criteria to distinguish between the algorithms within the NBCB and CBNB classes. In the first two rows of Table 4, we present which algorithms infer a WCG and which ones infer an ECG. In the next two rows, we detail the steps of the NBCB and CBNB classes of methods.

The next row indicates that NBCB-w and NBCB-e can still be applied even when Assumption 3 is violated. In such cases, the true graph may not be fully retrieved, but it is guaranteed that if the algorithms infer  $X \rightarrow Y$ , then in the true graph, we can be certain that  $Y \rightarrow X$ .

Similarly, the next row shows that CBNB-w and CBNB-e can be utilized even when Assumption 4 is violated. In this scenario, the true graph may not be completely retrieved, but the inferred graph’s skeleton will be accurate. The last three rows highlight the scenarios where each algorithm outperformed others. Interestingly, in the experimental section, we observed that methods inferring a WCG perform better with simulated data, while methods inferring an ECG excel with real data.

One of the key limitations of the CBNB and NBCB classes for real-world applications is their reliance on the restrictive assumption that there are no hidden confounders (Assumption 2), which could be often violated. For CBNB, we could consider an extension of the FRITL algorithm (Chen et al., 2021) for time-series, which is based on building the skeleton using FCI extension and refining after using noise-based methods. However, it is not clear how to adapt the necessary conditions for cyclic groups. For NBCB it could be more complicated to relax the no hidden confounders assumption.

Additionally, it would be interesting to adapt the CBNB and NBCB classes to the cases when there is a violation of consistency over time or stationarity. One potential direction could be to integrate our methods in the strategy proposed by Saggioro et al. (2020) which combines a causal discovery with a regime learning optimisation approach. However, this direction might require additional assumptions and while it appears promising for CBNB, it is less obvious for NBCB. Another direction could be to assume the presence of an observed contextual variable that explains the non-stationarity (Mooij et al., 2020, Günther et al., 2023).

Furthermore, adapting these methods for mixed data can be important in many applications. This can be straightforward for the constraint-based part of our algorithms, given the availability of conditional independence tests for mixed data (Zan et al., 2022). However, the adaptation is more challenging for the noise-based part.

Finally, although the framework we proposed does not necessitate a linearity assumption, our experimental section exclusively employed simulated linear data and utilized linear independence tests and linear regression models. Consequently, it would be compelling to explore our framework further by testing it on nonlinear simulated data in the future. This could involve employing nonlinear conditional independence tests and nonlinear regression models, considering that in many real-world scenarios, causal relations exhibit nonlinearity.

## 7 Conclusion

In this paper, we introduced a framework for hybrids of noise-based and constraint-based methods that can discover causal graphs from temporal data. Algorithms in the first class, denoted NBCB, start with ordering instantaneous relations, and then prune edges of the fully oriented graph. On the other hand, the algorithms from the second class, denoted CBNB, start by finding the skeleton and the orientation of lagged relations using a constraint-based method and temporal priority, then orient instantaneous relations by ordering nodes in each cycle group of instantaneous relations. Overall, the performance of our algorithms is a trade-off between the performance of constraint-based and noise-based algorithms when all assumptions are satisfied, and they outperform other methods in the cases where some of the assumptions are violated. For future works, it would be interesting to extend these approaches to cases involving hidden confounders, non-stationarity, and mixed data.

## References

- Andrew Arnold, Yan Liu, and Naoki Abe. Temporal causal modeling with graphical granger methods. In *Proceedings of the 13th ACM SIGKDD International Conference on Knowledge Discovery and Data Mining*, KDD ’07, pp. 66–75, New York, NY, USA, 2007. Association for Computing Machinery. ISBN 9781595936097. doi: 10.1145/1281192.1281203.
- Charles K. Assaad, Emilie Devijver, Eric Gaussier, and Ali Ait-Bachir. A mixed noise and constraint-based approach to causal inference in time series. In *Machine Learning and Knowledge Discovery in Databases. Research Track*, pp. 453–468, Cham, 2021. Springer International Publishing. ISBN 978-3-030-86486-6.



- Charles K. Assaad, Emilie Devijver, and Eric Gaussier. Survey and evaluation of causal discovery methods for time series. *J. Artif. Int. Res.*, 73, may 2022a. doi: 10.1613/jair.1.13428.
- Charles K. Assaad, Emilie Devijver, and Eric Gaussier. Entropy-based discovery of summary causal graphs in time series. *Entropy*, 24(8), 2022b. ISSN 1099-4300. doi: 10.3390/e24081156.
- Charles K. Assaad, Emilie Devijver, and Eric Gaussier. Discovery of extended summary graphs in time series. In James Cussens and Kun Zhang (eds.), *Proceedings of the Thirty-Eighth Conference on Uncertainty in Artificial Intelligence*, volume 180 of *Proceedings of Machine Learning Research*, pp. 96–106. PMLR, 01–05 Aug 2022c.
- Charles K. Assaad, Imad Ez-Zejjari, and Lei Zan. Root cause identification for collective anomalies in time series given an acyclic summary causal graph with loops. In Francisco Ruiz, Jennifer Dy, and Jan-Willem van de Meent (eds.), *Proceedings of The 26th International Conference on Artificial Intelligence and Statistics*, volume 206 of *Proceedings of Machine Learning Research*, pp. 8395–8404. PMLR, 25–27 Apr 2023.
- Frédéric Barraquand, Coralie Picoche, Matteo Detto, and Florian Hartig. Inferring species interactions using granger causality and convergent cross mapping. *Theoretical Ecology*, 14(1):87–105, 2021.
- Wei Chen, Kun Zhang, Ruichu Cai, Biwei Huang, Joseph Ramsey, Zhifeng Hao, and Clark Glymour. Fritl: A hybrid method for causal discovery in the presence of latent confounders. *arXiv preprint arXiv:2103.14238*, 2021.
- David Maxwell Chickering. Learning equivalence classes of bayesian-network structures. *J. Mach. Learn. Res.*, 2:445–498, mar 2002a. ISSN 1532-4435. doi: 10.1162/153244302760200696.
- David Maxwell Chickering. Optimal structure identification with greedy search. *Journal of machine learning research*, 3(Nov):507–554, 2002b.
- David Maxwell Chickering and Christopher Meek. Selective greedy equivalence search: Finding optimal bayesian networks using a polynomial number of score evaluations. *arXiv preprint arXiv:1506.02113*, 2015.
- Maria Dornelas, Laura H Antao, Faye Moyes, Amanda E Bates, Anne E Magurran, Dušan Adam, Asem A Akhmetzhanova, Ward Appeltans, Jose Manuel Arcos, Haley Arnold, et al. Biotime: A database of biodiversity time series for the anthropocene. *Global Ecology and Biogeography*, 27(7):760–786, 2018.
- Doris Entner and Patrik O Hoyer. On causal discovery from time series data using fci. *Probabilistic graphical models*, pp. 121–128, 2010.
- Chang Gong, Di Yao, Chuzhe Zhang, Wenbin Li, Jingping Bi, Lun Du, and Jin Wang. Causal discovery from temporal data. In *Proceedings of the 29th ACM SIGKDD Conference on Knowledge Discovery and Data Mining*, KDD ’23, pp. 5803–5804, New York, NY, USA, 2023. Association for Computing Machinery. ISBN 9798400701030. doi: 10.1145/3580305.3599552.
- Clive Granger. Investigating causal relations by econometric models and cross-spectral methods. *Econometrica*, 37(3):424–38, 1969.
- Clive W. J. Granger. Time series analysis, cointegration, and applications. *The American Economic Review*, 94(3):421–425, 2004. ISSN 00028282.
- Wiebke Günther, Urmi Ninad, and Jakob Runge. Causal discovery for time series from multiple datasets with latent contexts. In Robin J. Evans and Ilya Shpitser (eds.), *Proceedings of the Thirty-Ninth Conference on Uncertainty in Artificial Intelligence*, volume 216 of *Proceedings of Machine Learning Research*, pp. 766–776. PMLR, 31 Jul–04 Aug 2023.
- Uzma Hasan, Emam Hossain, and Md Osman Gani. A survey on causal discovery methods for iid and time series data. *Transactions on Machine Learning Research*, 2023.

- Patrik O. Hoyer, Aapo Hyvärinen, Richard Scheines, Peter L. Spirtes, Joseph Ramsey, Gustavo Lacerda, and Shohei Shimizu. Causal discovery of linear acyclic models with arbitrary distributions. In *Conference on Uncertainty in Artificial Intelligence*, 2008.
- Aapo Hyvärinen, Shohei Shimizu, and Patrik O. Hoyer. Causal modelling combining instantaneous and lagged effects: An identifiable model based on non-gaussianity. In *Proceedings of the 25th International Conference on Machine Learning, ICML '08*, pp. 424–431, New York, NY, USA, 2008. ACM. ISBN 978-1-60558-205-4.
- Christian Jost and Stephen P Ellner. Testing for predator dependence in predator-prey dynamics: a non-parametric approach. *Proceedings of the Royal Society of London. Series B: Biological Sciences*, 267(1453): 1611–1620, 2000.
- Yan Li, Rui Xia, Chunchen Liu, and Liang Sun. A hybrid causal structure learning algorithm for mixed-type data. In *Proceedings of the AAAI Conference on Artificial Intelligence*, volume 36, pp. 7435–7443, 2022.
- Daniel Malinsky and Peter Spirtes. Causal structure learning from multivariate time series in settings with unmeasured confounding. In *Proceedings of 2018 ACM SIGKDD workshop on causal discovery*, pp. 23–47. PMLR, 2018.
- Christopher Meek. Causal inference and causal explanation with background knowledge. In *Proceedings of the Eleventh Conference on Uncertainty in Artificial Intelligence, UAI'95*, pp. 403–410, San Francisco, CA, USA, 1995. Morgan Kaufmann Publishers Inc. ISBN 1558603859.
- Joris M. Mooij, Sara Magliacane, and Tom Claassen. Joint causal inference from multiple contexts. *Journal of Machine Learning Research*, 21(99):1–108, 2020.
- Mohammad Amin Morid, Olivia R Liu Sheng, and Joseph Dunbar. Time series prediction using deep learning methods in healthcare. *ACM Transactions on Management Information Systems*, 14(1):1–29, 2023.
- Juan Miguel Ogarrio, Peter Spirtes, and Joe Ramsey. A hybrid causal search algorithm for latent variable models. In *Conference on probabilistic graphical models*, pp. 368–379. PMLR, 2016.
- Roxana Pamfil, Nisara Sriwattanaworachai, Shaan Desai, Philip Pilgerstorfer, Konstantinos Georgatzis, Paul Beaumont, and Bryon Aragam. Dynotears: Structure learning from time-series data. In Silvia Chiappa and Roberto Calandra (eds.), *Proceedings of the Twenty Third International Conference on Artificial Intelligence and Statistics*, volume 108 of *Proceedings of Machine Learning Research*, pp. 1595–1605. PMLR, 26–28 Aug 2020.
- Keith Paton. An algorithm for finding a fundamental set of cycles of a graph. *Commun. ACM*, 12(9): 514–518, sep 1969. ISSN 0001-0782. doi: 10.1145/363219.363232.
- Judea Pearl. *Causality: Models, Reasoning, and Inference*. Cambridge University Press, New York, NY, USA, 2000. ISBN 0-521-77362-8.
- Jonas Peters, Joris M. Mooij, Dominik Janzing, and Bernhard Schölkopf. Identifiability of causal graphs using functional models. In *Proceedings of the Twenty-Seventh Conference on Uncertainty in Artificial Intelligence, UAI'11*, pp. 589–598, Arlington, Virginia, USA, 2011. AUAI Press. ISBN 9780974903972.
- Jonas Peters, Dominik Janzing, and Bernhard Schölkopf. Causal inference on time series using restricted structural equation models. In *Advances in Neural Information Processing Systems 26*, pp. 154–162, 2013.
- Jonas Peters, Joris M. Mooij, Dominik Janzing, and Bernhard Schölkopf. Causal discovery with continuous additive noise models. *Journal of Machine Learning Research*, 15(58):2009–2053, 2014.
- Jonas Peters, Dominik Janzing, and Bernhard Schölkopf. *Elements of Causal Inference: Foundations and Learning Algorithms*. The MIT Press, 2017. ISBN 0262037319.



## A Proofs

We recall the definition of blocked paths, backdoor paths, and the backdoor criterion.

**Definition 7** (Blocked path, Pearl, 2000). *A path is said to be blocked by a set of nodes  $\mathbb{S} \subset \mathbb{V}$  if it contains an intermediate cause or a common cause  $X$  such that  $X \in \mathbb{S}$  and if it contains a collider  $X$  such that  $X \notin \mathbb{S}$  and no descendant of  $X$  is in  $\mathbb{S}$ .*

Note that a path that is not blocked is said to be active.

**Definition 8** (Backdoor path, Pearl, 2000). *A path between an ordered pair  $(X, Y)$  is said to be a backdoor path between  $X$  and  $Y$  if it contains an arrow into  $X$ .*

Note that blocking all backdoor paths between two nodes eliminates confounding bias (Pearl, 2000).

**Theorem 1.** *Let  $\mathcal{G}^f = (\mathbb{V}^f, \mathbb{E}^f)$  be an FTCG. Under Assumptions 1, 2, 3, 4, 5, 6 and given perfect conditional independence information about all pairs of variables in  $\mathbb{V}^f$ , any algorithm in the NBCB class returns the correct WCG or the correct ECG compatible with  $\mathcal{G}^f$ .*

*Proof.* This proof is similar to the proof of Theorem 4 in Assaad et al. (2021) for NBCB<sup>acyclic</sup>. Given the Assumption 4 and causal sufficiency and assuming NB1 is consistent with Assumption 4, NB1 would infer the correct causal order  $\hat{\pi}$ . Given the causal order  $\hat{\pi}$  and temporal priority, we can orient all edges in a fully connected graph, which represents a super graph that contains the true graph. Given Assumptions 1, 2, 3, 6 and assuming that the constraint-based algorithm on which CB1' is based on is sound and complete, if we do not consider the causal order, CB1 would prune all unnecessary edges by removing edges between two nodes that are conditionally independent given a subset  $\mathbb{S}$  adjacent to one of these two nodes and yield the correct skeleton. Given the causal order  $\hat{\pi}$ , the subset  $\mathbb{S}$  can be reduced by containing only parents (instead of adjacencies). Thus, again by Assumptions 1, 2, 3, removing all edges between the conditionally independent nodes, the only edges that will be left with are causal, and so the graph would be correct.  $\square$

**Proposition 1** (Violation of Assumption 3). *Under Assumptions 1, 2, 4, 5, 6 and given a correct causal order between instantaneous nodes, the NBCB class would give WCGs and ECGs such that, for each pair of nodes  $X_{t^*}$  and  $Y_t$ , one of the following possibilities holds true:*

- (1) *The causal relationship between  $X_{t^*}$  and  $Y_t$  is correctly identified.*
- (2)  *$X_{t^*}$  and  $Y_t$  are not adjacent in the inferred graph, but they are adjacent in the true graph.*
- (3)  *$X_{t^*}$  and  $Y_t$  are adjacent in the inferred graph, but they are not adjacent in the true graph.*

*Proof.* Given that the noise-based algorithm on which the NB1 step is based on is correct, the NB1 step would give the correct causal order. Thus, having correct causal order for the instantaneous nodes and using orientation by time, the NB1 step would give the fully connected oriented graph, such that each edge that is present in the true graph is correctly oriented. The second step involves the CB1' step for pruning the edges. Since we consider that adjacency faithfulness is violated, we can have one of the following cases:

- If a pair of nodes  $X_{t^*}$  and  $Y_t$  is adjacent in the true graph there are two possible cases:
  - (a) there exist set  $\mathbb{S}$  such that  $X_{t^*} \perp\!\!\!\perp Y_t \mid \mathbb{S}$ . In this case, CB1' would erroneously remove the edge between  $X_{t^*}$  and  $Y_t$  in the inferred graph and we obtain case (2) in the proposition
  - (b) there exists no set  $\mathbb{S}$  such that  $X_{t^*} \perp\!\!\!\perp Y_t \mid \mathbb{S}$ , in this case, the CB1' would keep this edge and orientation of this edge is correct (given step NB1), this edge corresponds to correctly inferred causal relationship case (1)
- If a pair of nodes  $X_{t^*}$  and  $Y_t$  is not adjacent in the true graph but they are connected by an active path  $u = \langle X_{t^*}, V_{t_2^*}^2, \dots, V_{t_{n-1}^*}^{n-1}, Y_t \rangle$  of size  $n > 2$ . Suppose that due to violation of adjacency faithfulness, the step CB1' removes the edge  $X_{t^*} - V_{t_2^*}^2$  and the edge  $V_{t_{n-1}^*}^{n-1} - Y_t$ . If  $n = 3$ , then CB1' will never test if  $X_{t^*} \perp\!\!\!\perp Y_t \mid \mathbb{S}$ , such that  $V_{t_2^*}^2 \in \mathbb{S}$  therefore it will not remove the edge between  $X_{t^*}$  and  $Y_t$  in the inferred graph. If  $n > 3$  and if CB1' removes all possible edges between  $X_{t^*}$  and each node in  $\{V_{t_3^*}^3, \dots, V_{t_{n-1}^*}^{n-1}\}$  and all possible edges between  $Y_t$  and each node in  $\{V_{t_2^*}^2, \dots, V_{t_{n-2}^*}^{n-2}\}$  in

the inferred graph (due to a some specific configuration of the parameters that violates faithfulness but not adjacency faithfulness). Then, in this case, CB1' will never test if  $X_{t^*} \perp\!\!\!\perp Y_t \mid \mathbb{S}$ , such that  $\{V_{t_2}^2, \dots, V_{t_{n-1}}^{n-1}\} \cap \mathbb{S} = \emptyset$  therefore it will not remove the edge between  $X_{t^*}$  and  $Y_t$  in the inferred graph.

□

**Theorem 2.** *Let  $\mathcal{G}^f = (\mathbb{V}^f, \mathbb{E}^f)$  be an FTCTG. Under Assumptions 1, 2, 3, 4, 5, 6 and given perfect conditional independence information about all pairs of variables in  $\mathbb{V}^f$ , any algorithm in the CBNB class returns the correct WCG or the correct ECG compatible with  $\mathcal{G}^f$ .*

*Proof.* Without any given causal order, CB1 uses the first two steps of the constraint-based algorithm (omitting the orientation step). Using the full constraint-based algorithm under Assumptions 1, 2 and 3, we obtain correct partially complete partially oriented WCG or ECG  $\hat{\mathcal{G}}^*$ , i.e., correct skeleton, all instantaneous relations are not oriented and all lagged relations are oriented. So, having  $\hat{\mathcal{G}}^*$ , what is left to prove is that applying NB1' on the nodes  $\mathbb{I}_t$  that belong to each of undirected cyclic group  $\mathbb{C}$  given the past parents  $Pa_{\hat{\mathcal{G}}^*}(\mathbb{I}_t) \setminus \mathbb{V}_t$  is free of confounding bias.

To obtain the correct causal order  $\hat{\pi}$  between nodes  $\mathbb{I}_t$ , we need to verify that in the subgraph of  $\hat{\mathcal{G}}^*$  containing the nodes  $\mathbb{I}_t \cup Pa_{\hat{\mathcal{G}}^*}(\mathbb{I}_t)$  (which is by definition acyclic) for every two adjacent nodes  $X_t, Y_t \in \mathbb{I}_t$ , there exists a set  $\mathbb{S} \subseteq \mathbb{I}_t \setminus \{X_t, Y_t\} \cup Pa_{\hat{\mathcal{G}}^*}(\mathbb{I}_t)$ , such that  $\mathbb{S}$  blocks all backdoor paths between  $X_t$  and  $Y_t$  (if there is no edge between nodes  $X_t$  and  $Y_t$ , then there is no orientation to be determined by NB1'). Suppose  $X_t \rightarrow Y_t$  in the true graph (but in the output of CB1 this edge is unoriented) and there exists some active backdoor path  $u$  between  $X_t$  and  $Y_t$ , we consider two cases:

- (a) Suppose all nodes in path  $u$  belong to  $\mathbb{V}_t$ . By definition of an undirected cyclic group  $\mathbb{C}$ , all nodes in  $u$  are also in  $\mathbb{I}_t$ , which means that the common cause (common ancestor) on the path is also in  $\mathbb{I}_t$ , i.e., causal sufficiency is satisfied. This means, that  $u$  can be blocked by a node in  $\mathbb{I}_t$ . Thus there exists  $\mathbb{S} \subseteq \mathbb{I}_t \setminus \{X_t, Y_t\}$  such that all backdoor paths between  $X_t$  and  $Y_t$  are blocked.
- (b) Suppose that some nodes in  $u$  belong to  $\mathbb{V}^* \setminus \mathbb{V}_t$ . In this case, conditioning on  $Pa_{\hat{\mathcal{G}}^*}(\mathbb{I}_t)$  blocks  $u$  since  $Pa_{\hat{\mathcal{G}}^*}(\mathbb{I}_t)$  are the parents of  $\mathbb{I}_t$  and none of the nodes in  $Pa_{\hat{\mathcal{G}}^*}(\mathbb{I}_t)$  are colliders of any two nodes in  $\mathbb{I}_t$ . Thus all backdoor paths between  $X_t$  and  $Y_t$  passing by  $\mathbb{V}^* \setminus \mathbb{V}_t$  can be blocked by  $Pa_{\hat{\mathcal{G}}^*}(\mathbb{I}_t)$  and all the backdoor paths that are left are the ones discussed in (a).

□

**Proposition 2** (Violation of Assumption 4). *Under Assumptions 1, 2, 3, 5, 6 and given perfect conditional independence information about all pairs of variables, CBNB is guaranteed to find the correct skeleton of the WCG or the ECG.*

*Proof.* Given that the CB algorithm used for the CBNB method is correct under Assumptions 1 and 2, the result of the first step CB1 would give the correct skeleton under the Assumption 3. □

For example, if the PCMCi<sup>+</sup> method is used for the CBNB method, then the correctness of the skeleton comes from Theorem 1 in Runge (2020). In case when CB1 is based on PCGCE algorithm, the correctness of the skeleton is shown in Theorem 1 in Assaad et al. (2022c).

## B Pseudo-code algorithms

In our experimental section, we used an NB1 and an NB1' steps based on the VarLiNGAM algorithm (NB1 in NBCB-w and NBCB-e and NB1' in CBNB-w and CBNB-e) and we used respectively a CB1 and a CB1' steps based on the PCMCi<sup>+</sup> algorithm (CB1 in CBNB-w and CB1' in NBCB-w) and on the PCGCE algorithm (CB1 in CBNB-e and CB1' in NBCB-e). Since NB1' and CB' steps require more modifications compared to NB1 and CB1 steps starting from the initial methods, in the following, we provide the pseudo-codes of each NB' and CB' steps that we used. But first, we start by briefly recalling VarLiNGAM, PCMCi<sup>+</sup>, and PCGCE algorithms which all assume causal sufficiency (Assumption 2) while pointing out either their NB1 or CB1 step.



VarLiNGAM (Hyvärinen et al., 2008) is a noise-based causal discovery algorithm for time series data that constructs a WCG. First, it estimates a classic autoregressive model for the data using any conventional implementation of a least-squares method. It then computes the residuals and then performs the LiNGAM analysis (Shimizu et al., 2006; 2011) on the residuals. Note that the LiNGAM analysis can be either done using the ICALiNGAM (Shimizu et al., 2006) or DirectLiNGAM (Shimizu et al., 2011), in this work, we use DirectLiNGAM. This step, which we refer to as NB1, gives the causal order and the estimate of the instantaneous causal effects. After that, it computes the estimates of lagged causal effects. Finally, it estimates redundant directed edges to find the underlying WCG.

PCMCI<sup>+</sup> (Runge, 2020) is a constraint-based causal discovery algorithm for time series data that constructs a WCG. First, the PC1 lagged phase infers a superset of the lagged parents together with the parents of instantaneous ancestors. Next, the MCI instantaneous phase starts with links found in the previous step and all possible instantaneous links, then it conducts momentary conditional independence (MCI) with a modified conditioning set learned in the previous step to increase detection power. This step, which we refer to as CB1, gives a partially oriented graph where lagged relations are oriented and where instantaneous are non-oriented. Finally, it orients edges using the same rules used in the PC-algorithm (Spirtes et al., 2000, Meek, 1995).

Similarly, PCGCE (Assaad et al., 2022c) is also a constraint-based causal discovery algorithm for time series data, but that constructs an ECG without passing by a WCG. It also consists of two steps. First, it searches for the skeleton of the ECG using a procedure similar to the PC-algorithm that is order-independent by using a conditional independence test between either two nodes in the present slice or one node in the present slice and one node in the past slice, which can be multidimensional. Similarly to the case of PCMCI<sup>+</sup>, this step, which we refer to as CB1, gives a partially oriented graph where lagged relations are oriented and where instantaneous are non-oriented. Then it orients edges using the same rules used in the PC-algorithm (Spirtes et al., 2000, Meek, 1995).

In the following, we present the pseudo-codes of NB1' based on VarLiNGAM, CB1' based on PCMCI<sup>+</sup> and CB1' based on PCGCE. We colour in orange the parts that are different from the initial algorithms. Remark that the orange colour indicates that the corresponding parts are added or modified compared to the initial algorithms, but they do not indicate parts of the initial algorithms that were deleted.

### B.1 NB1' based on VarLiNGAM (Algorithm 3)

The NB1' step based on VarLiNGAM is almost identical to the NB1 step based on VarLiNGAM. As NB1, NB1' starts by computing the residuals of all instantaneous nodes by regressing them on their past. However, unlike NB1, NB1' focuses only on a subset of instantaneous nodes  $\mathbb{I}_t \subseteq \mathbb{V}_t$ . Note that also unlike NB1, NB1' takes as input a partially oriented graph  $\hat{\mathcal{G}}^*$  (the output of CB1 step which has the correct skeleton) and that  $\mathbb{I}_t \cup Pa_{\hat{\mathcal{G}}^*}(\mathbb{I}_t)$  should satisfy causal sufficiency. By construction, causal sufficiency is satisfied when  $\mathbb{I}_t$  is an undirected cycle group as defined in Definition 6. The pseudo-code of NB1' is provided in Algorithm 3.

### B.2 CB1' based on PCMCI<sup>+</sup> (Algorithm 4)

CB1 and CB1' based on the PCMCI<sup>+</sup> algorithm use conditional independence test  $CI()$  that returns at the same time the p-value and the statistic of the test. The main differences between the CB1' and the CB1 step based on PCMCI<sup>+</sup> is that CB1' takes a causal order as input, and therefore, it starts with a fully-oriented graph, in addition in the MCI instantaneous phase, it conditions only using parents (PCMCI<sup>+</sup> condition also on instantaneous adjacencies).

### B.3 CB1' based on PCGCE (Algorithm 5)

CB1 and CB1' based on the PCGCE algorithm use conditional independence test  $CI()$  that returns either the p-value of the test or the statistic without computing the p-value. The main difference between the CB1' and the CB1 step based on the PCGCE algorithm is that CB1' takes a causal order as input, and therefore, it starts with a fully-oriented graph and in addition, it conditions only using parents (PCGCE condition on adjacencies).

---

**Algorithm 3:** NB1' based on VarLiNGAM (parts in orange are different from the initial algorithms)

---

**Input:** A multivariate time series, a maximal temporal lag  $\gamma$ , a significance threshold  $\alpha$ , an independence measure  $I()$ , the output of the CB1 step  $\hat{\mathcal{G}}^*$  (partially oriented), and instantaneous nodes of interest  $\mathbb{I}_t \subseteq \mathbb{V}_t$

**Result:**  $\hat{\mathcal{G}}^*$  (fully oriented)

**if**  $\hat{\mathcal{G}}^*$  *is an ECG* **then**

Construct a WCG  $\mathcal{G}^w = (\mathbb{E}^w, \mathbb{V}^w = \{\mathbb{V}_{t-\gamma}, \dots, \mathbb{V}_t\})$  s.t.  $\forall X_{t-} \in \mathbb{V}_{t-}, Y_t \in \mathbb{V}_t$ , if  $X_{t-} \rightarrow Y_t \in \mathbb{E}^e$  then  $\forall \ell \in \{1, \dots, \gamma\}$ ,  $X_{t-\ell} \rightarrow Y_t \in \mathbb{E}^w$  and  $\forall X_t, Y_t \in \mathbb{V}_t$  if  $X_t \neq Y_t$ ,  $X_t \rightarrow Y_t \in \mathbb{E}^e$  then  $X_t \neq Y_t$ ,  $X_t \rightarrow Y_t \in \mathbb{E}^w$ ;

**else**

$\hat{\mathcal{G}}^w = \hat{\mathcal{G}}^*$ ;

**for**  $Y_t \in \mathbb{I}_t$  **do**

Estimate a classic autoregressive model for the data

$$Y_t = \sum_{X_{t-\ell} \in Pa_{\hat{\mathcal{G}}^w}(\mathbb{I}_t)} a_{xy\ell} X_{t-\ell} + \xi_t^y$$

using any conventional implementation of a least-squares method. Note that here  $\ell > 0$ , so it is really a classic AR model;

Compute the residuals, that is, estimates of  $\xi_t^y$ ;

$$\hat{\xi}_t^y = Y_t - \sum_{X_{t-\ell} \in Pa_{\hat{\mathcal{G}}^w}(\mathbb{I}_t)} \hat{a}_{xy\ell} X_{t-\ell}$$

Initialize a bijective mapping function  $\pi$ ;

$i = 1$ ;

Initialize a list  $\mathbb{S}$  containing all nodes in  $\mathbb{I}_t$ ;

**while**  $\text{size}(\mathbb{S}) > 1$  **do**

Initialize an empty list  $\mathbb{H}$ ;

**for**  $X_t \in \mathbb{S}$  **do**

**for**  $Y_t \in \mathbb{S} \setminus \{X_t\}$  **do**

Perform least squares regressions of  $\hat{\xi}_t^x$  on  $\hat{\xi}_t^y$  and compute the residuals:

$$\hat{\epsilon}^{Y_t} = \hat{\xi}_t^y - \frac{\text{cov}(\hat{\xi}_t^x, \hat{\xi}_t^y)}{\text{var}(\hat{\xi}_t^x)}$$

Estimate the dependence between the total residuals and  $X_t$ :

$$h = \sum_{Y_t \in \mathbb{S} \setminus \{X_t\}} I(\hat{\xi}_t^x, \hat{\epsilon}^{Y_t})$$

Append  $h$  to the end of  $\mathbb{H}$ ;

Find the node  $X_t$  corresponding to  $\hat{\xi}_t^x$  that is most independent of its residuals in  $\mathbb{H}$ ;

$\pi(X_t) = i$ ;

$i = i + 1$ ;

Remove  $X_t$  from  $\mathbb{S}$ ;

$\pi(X_t) = i$  where  $X_t$  is the remaining instantaneous node in  $\mathbb{S}$ ;

**Orient**  $\hat{\mathcal{G}}^*$  s.t.  $\forall X_t - Y_t \in \mathbb{E}^*$ ,  $X_t \rightarrow Y_t \in \mathbb{E}^*$  if  $\pi(X_t) < \pi(Y_t)$ ;

---

---

**Algorithm 4:** CBI' based on PCMCI<sup>+</sup> (parts in orange are different from the initial algorithms)

---

**Input:** A multivariate time series, a maximal temporal lag  $\gamma$  and a significance threshold  $\alpha$ , a conditional independence test  $CI()$ , and a causal order  $\pi$

**Result:**  $\mathcal{G}^w$  (WCG)

Construct an fully-connected WCG  $\mathcal{G}^w = (\mathbb{E}^w, \mathbb{V}^w = \{\mathbb{V}_{t-\gamma}, \dots, \mathbb{V}_t\})$  s.t.

$\forall X_{t-\ell} \in \{\mathbb{V}_{t-\gamma}, \dots, \mathbb{V}_{t-1}\}, Y_t \in \mathbb{V}_t, X_{t-\ell} \rightarrow Y_t \in \mathbb{E}^w$  and  $\forall X_t, Y_t \in \mathbb{V}_t$  s.t.  $X_t \neq Y_t, X_t \rightarrow Y_t \in \mathbb{E}^w$  if  $\pi(X_t) < \pi(Y_t)$ ;

for  $Y_t \in \mathbb{V}_t$  do

    Initialize  $\hat{B}_t(Y_t) = \mathbb{V}^w \setminus \mathbb{V}_t$ ;

    Initialize  $I^{\min}(X_{t-\ell}, Y_t) = \infty \forall X_{t-\ell} \in \hat{B}_t(Y_t)$ ;

$n = 0$ ;

    while  $\exists X_{t-\ell} \in \hat{B}_t(Y_t)$  s.t.  $\text{size}(\hat{B}_t(Y_t)) \geq n$  do

        for  $X_{t-\ell} \in \mathbb{V}^w \setminus \mathbb{V}_t$  s.t.  $\text{size}(\hat{B}_t(Y_t)) \geq n$  do

$\mathbb{S} =$  first  $n$  nodes in  $\hat{B}_t(Y_t)$ ;

$p, h = CI(X_{t-\ell}, Y_t \mid \mathbb{S})$ ;

$I^{\min}(X_{t-\ell}, Y_t) = \min(|h|, I^{\min}(X_{t-\ell}, Y_t))$ ;

            if  $p > \alpha$  then

                mark  $X_{t-\ell}$  for removal

$\forall X_{t-\ell}$  marked for removal, remove  $X_{t-\ell} \rightarrow Y_t$  from  $\mathbb{E}^w$ ;

        Sort  $\hat{B}_t(Y_t)$  by  $I^{\min}(X_{t-\ell}, Y_t)$  from largest to smallest;

$n = n + 1$ ;

Initialize  $I^{\min}(X_{t-\ell}, Y_t) = \infty \forall X_{t-\ell} \in \hat{B}_t(Y_t)$ ;

$n = 0$ ;

while  $\exists X_{t-\ell} - Y_t \in \mathbb{E}^w \forall \ell \geq 0$  s.t.  $\text{size}(Pa_{\hat{\mathcal{G}}^w}(Y_t) \cap \mathbb{V}_t \setminus \{X_{t-\ell}\}) \geq n$  do

    for  $X_{t-\ell} - Y_t \in \mathbb{E}^w \forall \ell \geq 0$  s.t.  $\text{size}(Pa_{\hat{\mathcal{G}}^w}(Y_t) \cap \mathbb{V}_t \setminus \{X_{t-\ell}\}) \geq n$  do

        while  $\exists X_{t-\ell} - Y_t \in \mathbb{E}^w$  and not all  $\mathbb{S} \in Pa_{\hat{\mathcal{G}}^w}(Y_t) \cap \mathbb{V}_t \setminus \{X_{t-\ell}\}$  with  $\text{size}(\mathbb{S}) = n$  have been considered do

            for  $\mathbb{S} \in Pa_{\hat{\mathcal{G}}^w}(Y_t) \cap \mathbb{V}_t \setminus \{X_{t-\ell}\}$  s.t.  $\text{size}(\mathbb{S}) = n$  do

$p, h = CI(Y_t, X_{t-\ell} \mid \mathbb{S}, \hat{B}_t(Y_t) \setminus \{X_{t-\ell}\}, \hat{B}_{t-\ell}(X_{t-\ell}))$ ;

$I^{\min}(X_{t-\ell}, Y_t) = \min(|h|, I^{\min}(X_{t-\ell}, Y_t))$ ;

                if  $p > \alpha$  then

                    Remove  $X_{t-\ell} \rightarrow Y_t$  from  $\mathbb{E}^w$  or  $X_{t-\ell} - Y_t$  from  $\mathbb{E}^w$ ;

$n = n + 1$ ;

    Sort  $Pa_{\hat{\mathcal{G}}^w}(Y_t) \cap \mathbb{V}_t$  by  $I^{\min}(X_{t-\ell}, Y_t)$  from largest to smallest;

---

---

**Algorithm 5:** CB1' based on PCGCE (parts in orange are different from the initial algorithms)

---

**Input:** A multivariate time series, a maximal temporal lag  $\gamma$  and a significance threshold  $\alpha$ , a conditional independence test  $CI()$ , and a causal order  $\pi$

**Result:**  $\mathcal{G}^e$  (ECG)

Construct an fully-connected ECG  $\mathcal{G}^e = (\mathbb{E}^e, \mathbb{V}^e = \{\mathbb{V}_{t-}, \mathbb{V}_t\})$  s.t.  $\forall X_{t-} \in \mathbb{V}_{t-}, Y_t \in \mathbb{V}_t, X_{t-} \rightarrow Y_t \in \mathbb{E}^e$  and  $\forall X_t, Y_t \in \mathbb{V}_t$  s.t.  $X_t \neq Y_t, X_t \rightarrow Y_t \in \mathbb{E}^e$  if  $\pi(X_t) < \pi(Y_t)$  ;

$n = 0$ ;

```

while  $\exists X_{t*} - Y_t \in \mathbb{E}^e \forall t* \in \{t, t-\}$  s.t.  $\text{size}(Pa_{\hat{\mathcal{G}}^e}(Y_t) \setminus \{X_{t*}\}) \geq n$  do
  Initialize  $\mathbb{D}$  and  $\mathbb{H}$  as empty lists;
  for  $X_{t*} - Y_t \in \mathbb{E}^e \forall t* \in \{t, t-\}$  s.t.  $\text{size}(Pa_{\hat{\mathcal{G}}^e}(Y_t) \setminus \{X_{t*}\}) = n$  do
    while  $\exists X_{t*} - Y_t \in \mathbb{E}^e$  and not all  $\mathbb{S} \in Pa_{\hat{\mathcal{G}}^e}(Y_t) \setminus \{X_{t*}\}$  with  $\text{size}(\mathbb{S}) = n$  have been considered do
      for  $\mathbb{S} \subset Pa_{\hat{\mathcal{G}}^e}(Y_t) \setminus \{X_{t*}\}$  s.t.  $\text{size}(\mathbb{S}) = n$  do
         $-, h = CI(X_{t*}, Y_t \mid \mathbb{S})$ ;
        Save  $(X_{t*}, Y_t, \mathbb{S})$  in  $\mathbb{D}$  and  $h$  in  $\mathbb{H}$ 
      end for
    end while
  end for
  Sort  $\mathbb{D}$  and  $\mathbb{H}$  by  $\mathbb{H}$  from smallest to largest;
  for  $X_{t*}, Y_t, \mathbb{S} \in \mathbb{D}$  s.t.  $\mathbb{S} \subseteq Pa_{\hat{\mathcal{G}}^e}(Y_t)$  do
     $p, - = CI(X_{t*}, Y_t \mid \mathbb{S})$ ;
    if  $p > \alpha$  then
      Remove  $X_{t*} \rightarrow Y_t$  from  $\mathbb{E}^e$  or  $X_{t*} - Y_t$  from  $\mathbb{E}^e$ ;
    end if
  end for
   $n = n + 1$ ;

```

---

## C Experimental setup

Time series in monitoring systems are not always exactly aligned together and come in different sampling rates as the timestamps depend on when the data was collected. In the following, we present two pre-processing strategies that we considered for aligning time series:

- Strategy 1: Time series are analyzed in terms of sampling rates and the lowest one is chosen. Afterwards, all the time series are re-sampled according to this lowest sampling rate with the closest value to the timestamp taken as the new value. Upon re-sampling, missing values can be clearly observed. If missing values are detected, they are filled using simple linear interpolation of Pandas data frames<sup>7</sup>.
- Strategy 2: Each raw value  $x_i$  is converted into integral value  $s_i$  at each point  $i$  as follows:  $s_i = x_i(t_i - t_{i-1}) + s_{i-1}$ . Then all time series are re-sampled such that each re-sampled value  $x_j$  at every  $n$  (the lowest sampling rate) steps is calculated as follows:  $x_j = \frac{s_i - s_{i-n}}{t_i - t_{i-n}}$ . The time  $t_i$  (of value  $s_i$ ) is the time that is after the corresponding time to  $x_j$ .

## D Links to datasets

**Temperature.** Available at <https://webdav.tuebingen.mpg.de/cause-effect/>.

**Veilleux.** Available at <http://robjhyndman.com/tsdldata/data/veilleux.dat>.

**Diary.** Available at <http://future.aae.wisc.edu>.

**Ingestion mini.** Available at [https://easyvista2015-my.sharepoint.com/personal/aait-bachir\\_easyvista\\_com/\\_layouts/15/onedrive.aspx?id=%2Fpersonal%2Faait%2Dbachir%5Feasyvista%5Fcom%2FDocuments%2FLab%2FPublicData&ga=1](https://easyvista2015-my.sharepoint.com/personal/aait-bachir_easyvista_com/_layouts/15/onedrive.aspx?id=%2Fpersonal%2Faait%2Dbachir%5Feasyvista%5Fcom%2FDocuments%2FLab%2FPublicData&ga=1).

**Web.** Available at [https://easyvista2015-my.sharepoint.com/personal/aait-bachir\\_easyvista\\_com/\\_layouts/15/onedrive.aspx?id=%2Fpersonal%2Faait%2Dbachir%5Feasyvista%5Fcom%2FDocuments%2FLab%2FPublicData&ga=1](https://easyvista2015-my.sharepoint.com/personal/aait-bachir_easyvista_com/_layouts/15/onedrive.aspx?id=%2Fpersonal%2Faait%2Dbachir%5Feasyvista%5Fcom%2FDocuments%2FLab%2FPublicData&ga=1).

<sup>7</sup><https://pandas.pydata.org/docs/reference/api/pandas.DataFrame.interpolate.html>

**Antivirus.** Available at [https://easyvista2015-my.sharepoint.com/personal/aait-bachir\\_easyvista\\_com/\\_layouts/15/onedrive.aspx?id=%2Fpersonal%2Faat%2Dbachir%5Feasyvista%5Fcom%2FDocuments%2FLab%2FPublicData&ga=1](https://easyvista2015-my.sharepoint.com/personal/aait-bachir_easyvista_com/_layouts/15/onedrive.aspx?id=%2Fpersonal%2Faat%2Dbachir%5Feasyvista%5Fcom%2FDocuments%2FLab%2FPublicData&ga=1).

## E Additional experiments

In Table 5 we provide F1 score on the adjacencies. In contrast to Table 1 in the main text, this Table shows the performance of the algorithms on skeleton recovery which allows to illustrate the robustness of CBNB class to Assumption 4.

Table 5: Results obtained on the simulated data of Section 5.2 for the different structures with 1000 observations with non-Gaussian noise (top panel) and with Gaussian noise (bottom panel). We report the mean and the standard deviation of the F1 score on adjacencies. The best results are in blue bold and the second best results are in green bold.

	Diamond	Cyclic Diamond	Unf. Diamond	Adj. Unf. Diamond
Non-Gaussian noise				
NBCB-w	<b>0.95</b> $\pm$ 0.01	0.95 $\pm$ 0.01	0.94 $\pm$ 0.01	<b>0.88</b> $\pm$ 0.01
CBNB-w	<b>0.95</b> $\pm$ 0.01	<b>0.96</b> $\pm$ 0.01	0.95 $\pm$ 0.01	<b>0.88</b> $\pm$ 0.01
NBCB-e	0.86 $\pm$ 0.01	0.85 $\pm$ 0.01	<b>0.97</b> $\pm$ 0.01	<b>0.87</b> $\pm$ 0.01
CBNB-e	0.85 $\pm$ 0.01	0.86 $\pm$ 0.01	<b>0.97</b> $\pm$ 0.01	<b>0.87</b> $\pm$ 0.01
GCMVL	0.87 $\pm$ 0.01	0.92 $\pm$ 0.01	0.07 $\pm$ 0.01	0.06 $\pm$ 0.02
PCMCI <sup>+</sup>	<b>0.95</b> $\pm$ 0.01	<b>0.96</b> $\pm$ 0.01	0.95 $\pm$ 0.04	<b>0.88</b> $\pm$ 0.01
PCCGE	0.85 $\pm$ 0.01	0.86 $\pm$ 0.01	<b>0.97</b> $\pm$ 0.01	<b>0.87</b> $\pm$ 0.01
Dynotears	0.09 $\pm$ 0.03	0.0 $\pm$ 0.0	0.0 $\pm$ 0.0	0.0 $\pm$ 0.0
VarLiNGAM	<b>0.99</b> $\pm$ 0.01	<b>0.97</b> $\pm$ 0.01	<b>0.98</b> $\pm$ 0.01	<b>0.87</b> $\pm$ 0.01
Gaussian noise				
NBCB-w	<b>0.93</b> $\pm$ 0.01	<b>0.93</b> $\pm$ 0.01	0.90 $\pm$ 0.01	<b>0.87</b> $\pm$ 0.01
CBNB-w	<b>0.96</b> $\pm$ 0.01	<b>0.96</b> $\pm$ 0.01	<b>0.94</b> $\pm$ 0.01	<b>0.87</b> $\pm$ 0.01
NBCB-e	0.83 $\pm$ 0.01	0.83 $\pm$ 0.01	0.93 $\pm$ 0.01	<b>0.85</b> $\pm$ 0.01
CBNB-e	0.85 $\pm$ 0.01	0.84 $\pm$ 0.01	<b>0.97</b> $\pm$ 0.01	<b>0.87</b> $\pm$ 0.01
GCMVL	0.88 $\pm$ 0.01	0.91 $\pm$ 0.01	0.02 $\pm$ 0.01	0.03 $\pm$ 0.01
PCMCI <sup>+</sup>	<b>0.96</b> $\pm$ 0.01	<b>0.96</b> $\pm$ 0.01	<b>0.94</b> $\pm$ 0.01	<b>0.87</b> $\pm$ 0.01
PCCGE	0.85 $\pm$ 0.01	0.84 $\pm$ 0.01	<b>0.97</b> $\pm$ 0.01	<b>0.87</b> $\pm$ 0.01
Dynotears	0.13 $\pm$ 0.05	0.0 $\pm$ 0.0	0.0 $\pm$ 0.0	0.0 $\pm$ 0.0
VarLiNGAM	0.91 $\pm$ 0.01	0.92 $\pm$ 0.01	0.93 $\pm$ 0.01	0.84 $\pm$ 0.01